Today's Outline - November 02, 2016

Today's Outline - November 02, 2016

- X-ray absorption spectroscopy

Today's Outline - November 02, 2016

- X-ray absorption spectroscopy
- EXAFS of NFA steels

Today's Outline - November 02, 2016

- X-ray absorption spectroscopy
- EXAFS of NFA steels
- In situ EXAFS studies

Today's Outline - November 02, 2016

- X-ray absorption spectroscopy
- EXAFS of NFA steels
- In situ EXAFS studies
- Angle Resolved Photoemission

Today's Outline - November 02, 2016

- X-ray absorption spectroscopy
- EXAFS of NFA steels
- In situ EXAFS studies
- Angle Resolved Photoemission
- Resonant Scattering

Today's Outline - November 02, 2016

- X-ray absorption spectroscopy
- EXAFS of NFA steels
- In situ EXAFS studies
- Angle Resolved Photoemission
- Resonant Scattering

Homework Assignment #05:
Chapter 5: 1, 3, 7, 9, 10
due Monday, November 07, 2016

Today's Outline - November 02, 2016

- X-ray absorption spectroscopy
- EXAFS of NFA steels
- In situ EXAFS studies
- Angle Resolved Photoemission
- Resonant Scattering

Homework Assignment #05:
Chapter 5: 1, 3, 7, 9, 10
due Monday, November 07, 2016

Homework Assignment #06:
Chapter 6: 1,6,7,8,9
due Monday, November 14, 2016

Today's Outline - November 02, 2016

- X-ray absorption spectroscopy
- EXAFS of NFA steels
- In situ EXAFS studies
- Angle Resolved Photoemission
- Resonant Scattering

Homework Assignment #05:
Chapter 5: 1, 3, 7, 9, 10
due Monday, November 07, 2016

Homework Assignment #06:
Chapter 6: 1,6,7,8,9
due Monday, November 14, 2016

No class on Wednesday, November 09, 2016

X-ray absorption by a free atom

An atom absorbs an x-ray of energy E, destroying a core electron with energy E_0 and creating a photo-electron with energy $(E - E_0)$. The core hole is eventually filled, and a fluorescence x-ray or Auger electron is ejected from the atom.

X-ray absorption by a free atom

An atom absorbs an x-ray of energy E, destroying a core electron with energy E_0 and creating a photo-electron with energy $(E - E_0)$. The core hole is eventually filled, and a fluorescence x-ray or Auger electron is ejected from the atom.

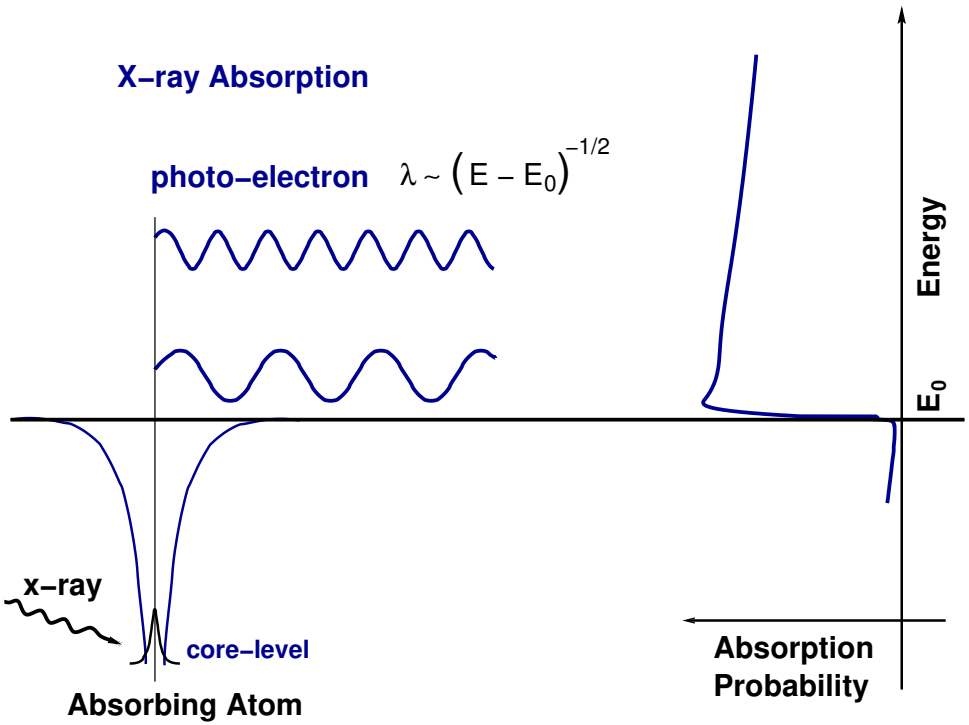

X-ray absorption by a free atom

An atom absorbs an x-ray of energy E, destroying a core electron with energy E_0 and creating a photo-electron with energy $(E - E_0)$. The core hole is eventually filled, and a fluorescence x-ray or Auger electron is ejected from the atom.

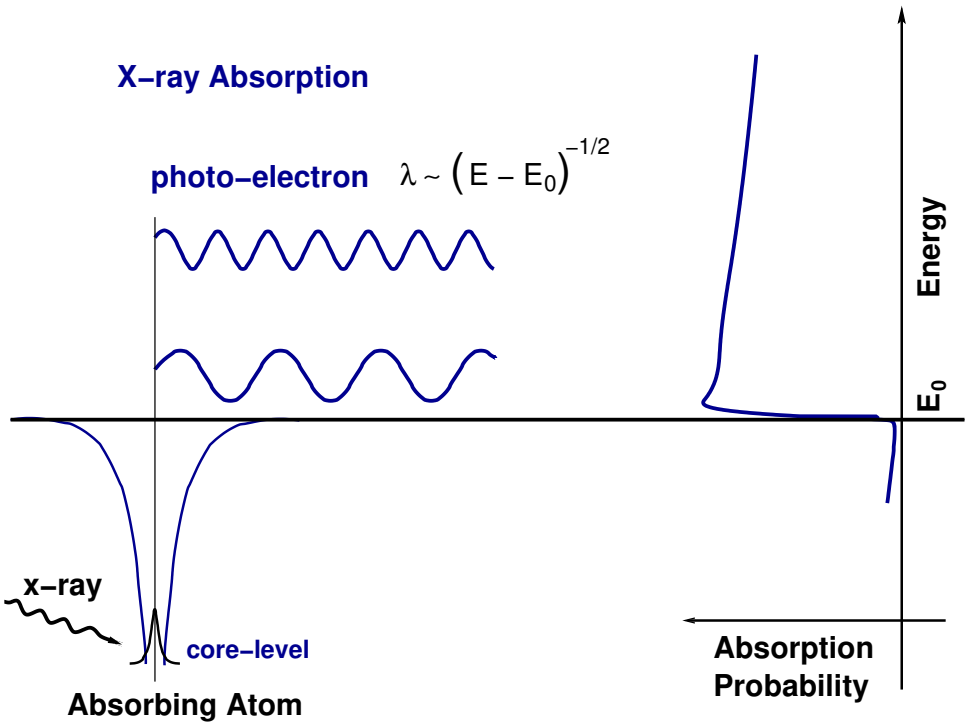

x-ray absorption needs an available state for the photo-electron to go into

X-ray absorption by a free atom

An atom absorbs an x-ray of energy E, destroying a core electron with energy E_0 and creating a photo-electron with energy $(E - E_0)$. The core hole is eventually filled, and a fluorescence x-ray or Auger electron is ejected from the atom.

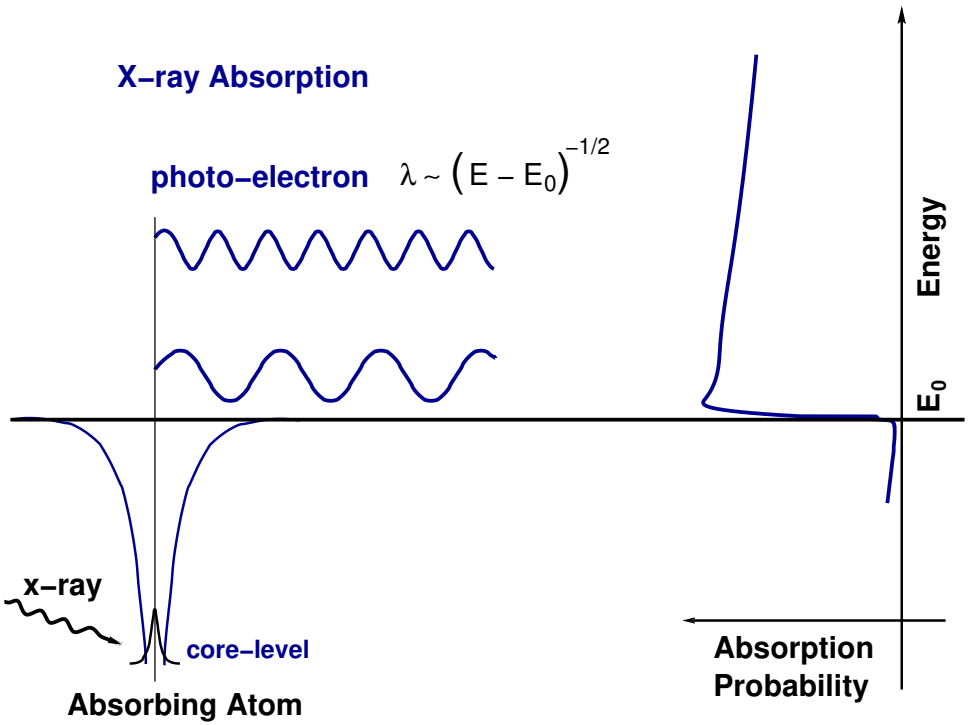

x-ray absorption needs an available state for the photo-electron to go into

No available state:
No absorption

X-ray absorption by a free atom

An atom absorbs an x-ray of energy E, destroying a core electron with energy E_0 and creating a photo-electron with energy $(E - E_0)$. The core hole is eventually filled, and a fluorescence x-ray or Auger electron is ejected from the atom.

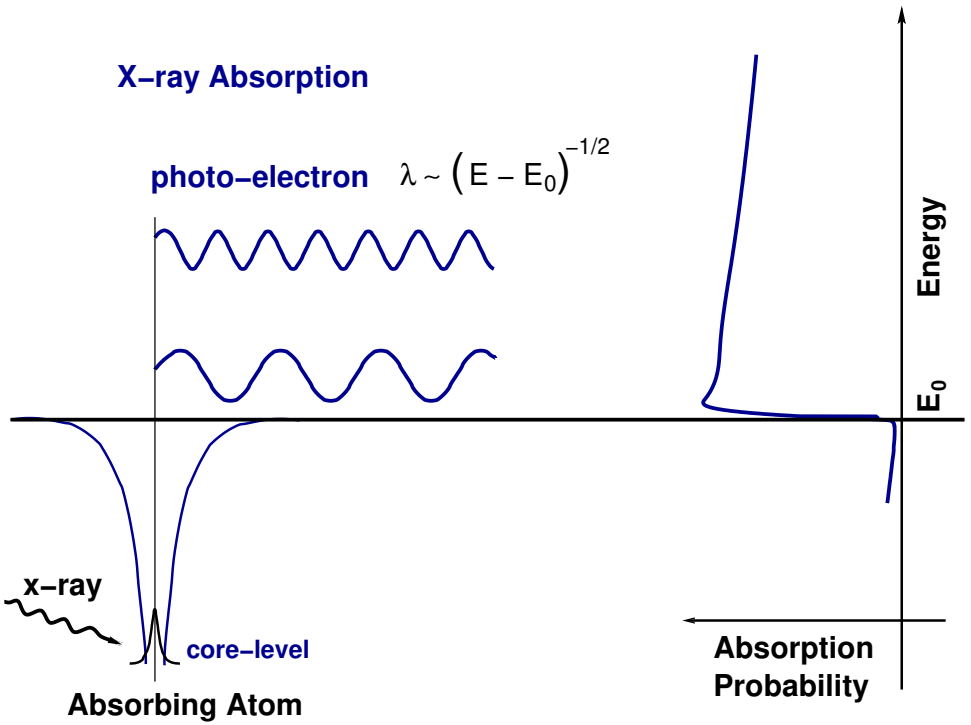

x-ray absorption needs an available state for the photo-electron to go into

No available state:
No absorption

Once the x-ray energy is large enough to promote a core-level to the continuum, there is a sharp increase in absorption.

X-ray absorption by a free atom

An atom absorbs an x-ray of energy E, destroying a core electron with energy E_0 and creating a photo-electron with energy $(E - E_0)$. The core hole is eventually filled, and a fluorescence x-ray or Auger electron is ejected from the atom.

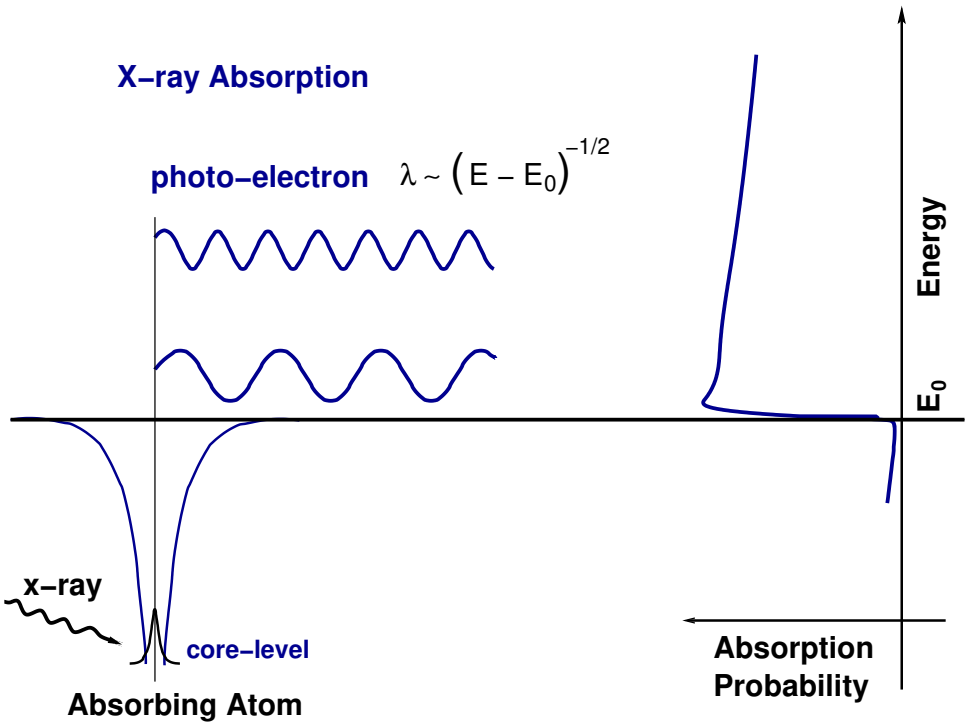

x-ray absorption needs an available state for the photo-electron to go into

No available state:
No absorption

Once the x-ray energy is large enough to promote a core-level to the continuum, there is a sharp increase in absorption.

$\mu(E)$ has a sharp step at the core-level binding energy, and is a smooth function of energy above this absorption edge.

X-ray absorption with photo-electron scattering

With another atom nearby, the ejected photo-electron can *scatter* from a neighboring atom and return back to the absorbing atom.

X-ray absorption with photo-electron scattering

With another atom nearby, the ejected photo-electron can *scatter* from a neighboring atom and return back to the absorbing atom.

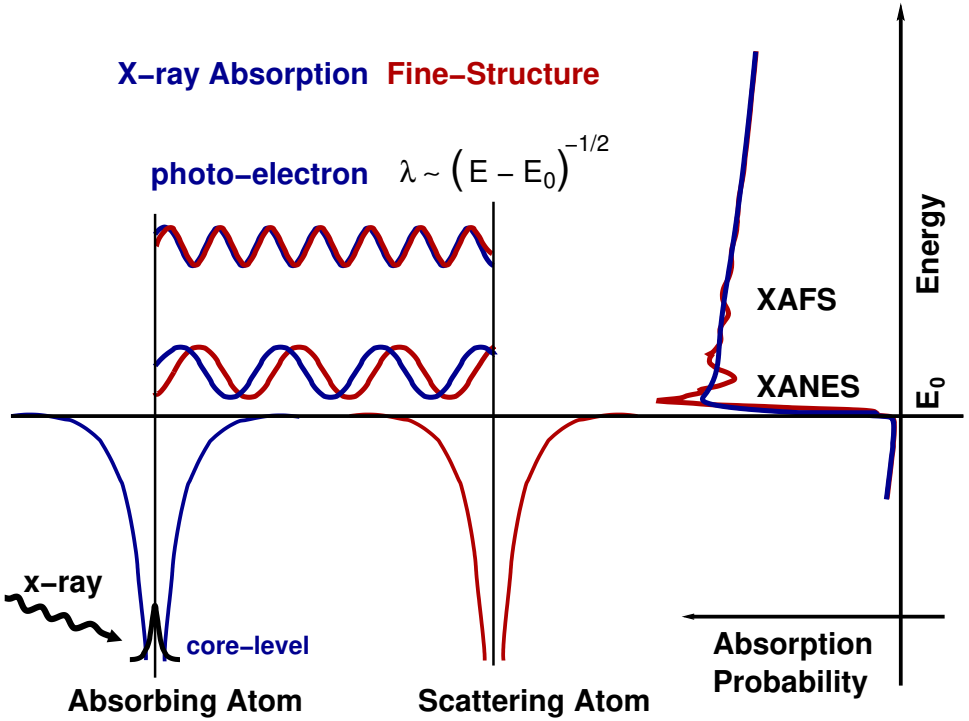

X-ray absorption with photo-electron scattering

With another atom nearby, the ejected photo-electron can *scatter* from a neighboring atom and return back to the absorbing atom.

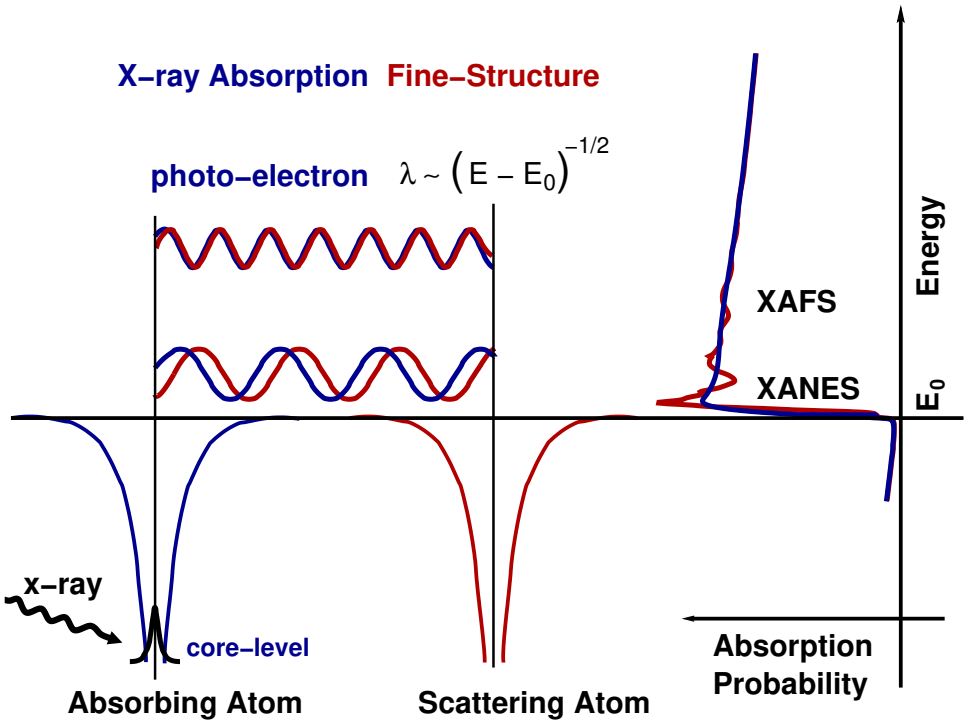

The photo-electron scattered back will interfere with itself.

μ depends on the presence of an electron state with energy $(E - E_0)$, at the absorbing atom.

X-ray absorption with photo-electron scattering

With another atom nearby, the ejected photo-electron can *scatter* from a neighboring atom and return back to the absorbing atom.

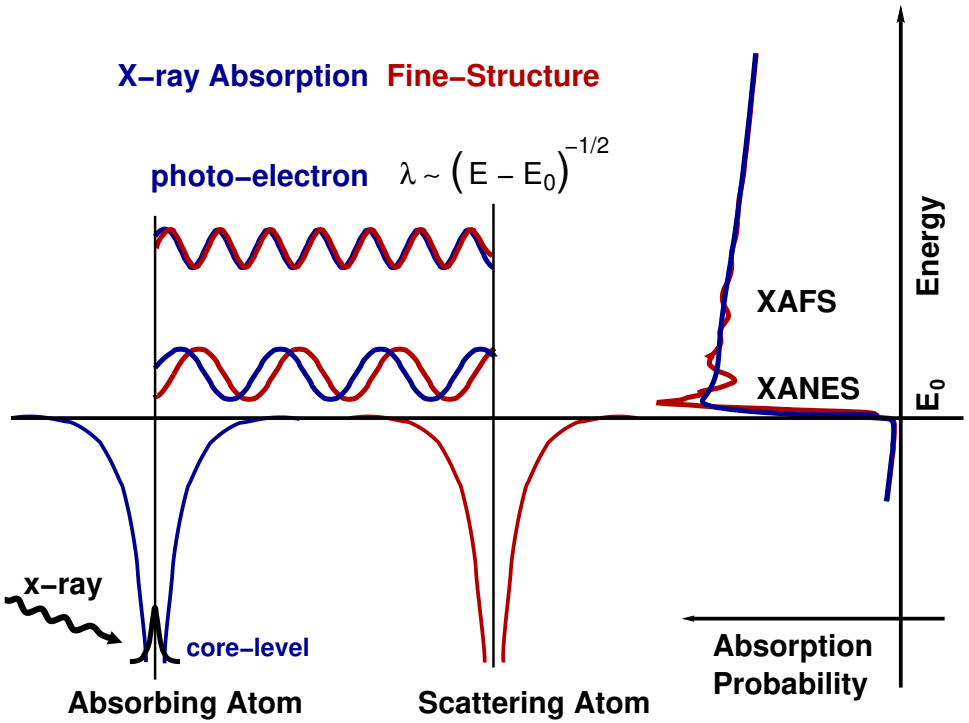

The photo-electron scattered back will interfere with itself.

μ depends on the presence of an electron state with energy $(E - E_0)$, at the absorbing atom.

The amplitude of the back-scattered photo-electron *at the absorbing atom* will vary with energy, causing the oscillations in $\mu(E)$ that are the XAFS. The XAFS oscillations are an interference effect of the photo-electron with itself, due to the presence of neighboring atoms.

X-ray absorption: Fermi's golden rule

$$\mu(E) = \mu_0(E)[1 + \chi(E)]$$

X-ray absorption: Fermi's golden rule

$$\mu(E) = \mu_0(E)[1 + \chi(E)]$$

$$\chi(k[E]) = \frac{\mu(E) - \mu_0(E)}{\mu_0(E)}$$

X-ray absorption: Fermi's golden rule

$$\mu(E) = \mu_0(E)[1 + \chi(E)]$$

$$\chi(k[E]) = \frac{\mu(E) - \mu_0(E)}{\mu_0(E)}$$

$$k = \sqrt{\frac{2m(E - E_0)}{\hbar^2}}$$

X-ray absorption: Fermi's golden rule

$$\mu(E) = \mu_0(E)[1 + \chi(E)]$$

$$\chi(k[E]) = \frac{\mu(E) - \mu_0(E)}{\mu_0(E)}$$

$$k = \sqrt{\frac{2m(E - E_0)}{\hbar^2}}$$

$$\mu(E) \sim |\langle i|\mathcal{H}|f\rangle|^2$$

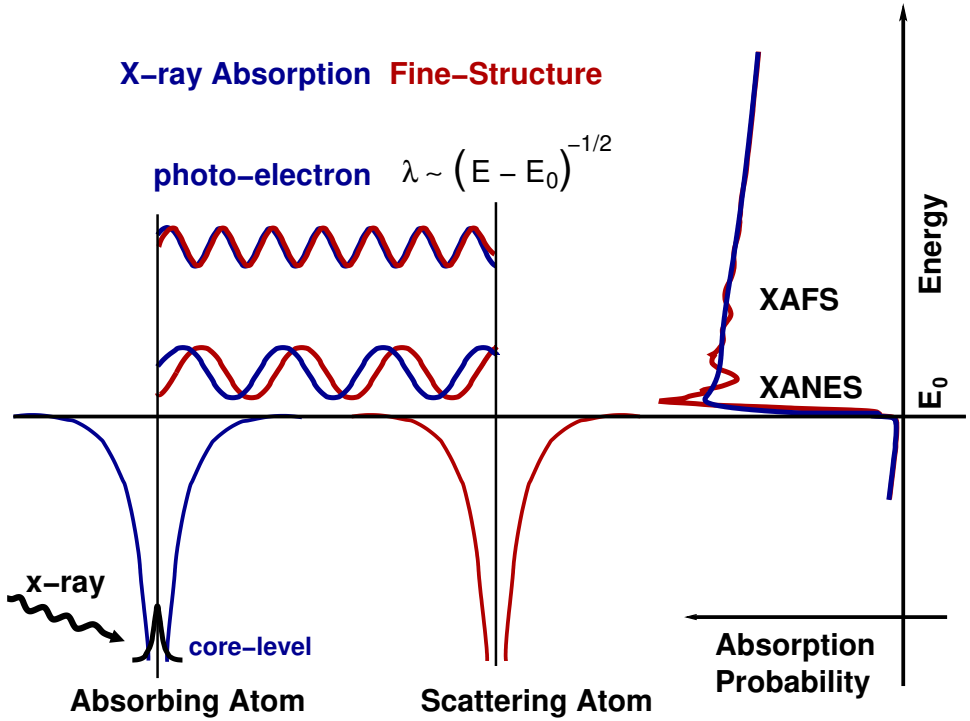

X-ray absorption: Fermi's golden rule

$$\mu(E) = \mu_0(E)[1 + \chi(E)]$$

$$\chi(k[E]) = \frac{\mu(E) - \mu_0(E)}{\mu_0(E)}$$

$$k = \sqrt{\frac{2m(E - E_0)}{\hbar^2}}$$

$$\mu(E) \sim |\langle i|\mathcal{H}|f\rangle|^2$$

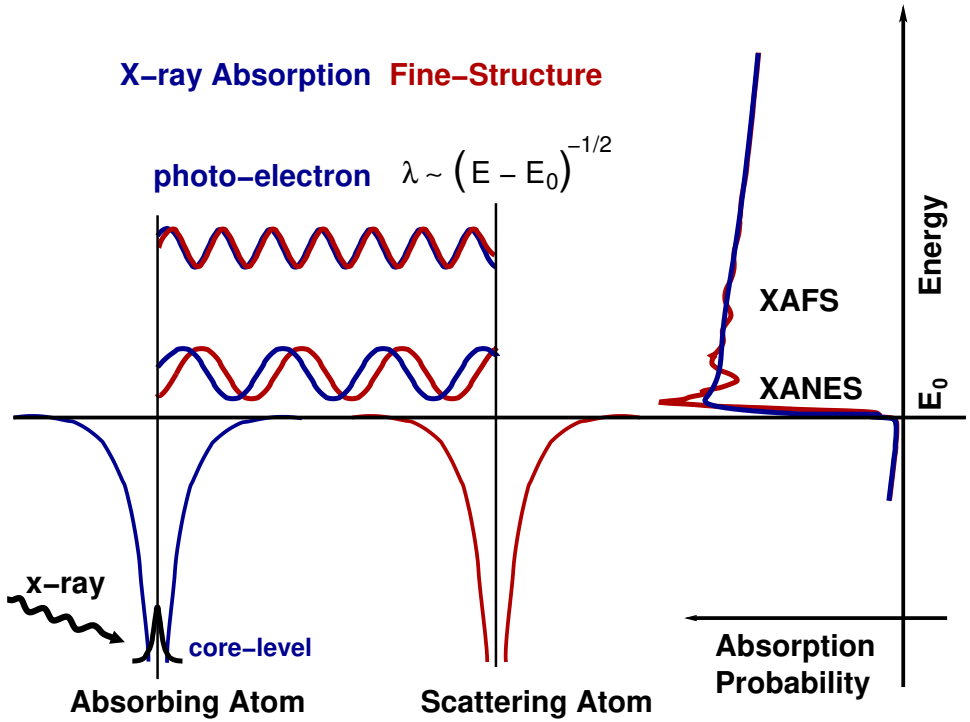

$\langle i|$ the *initial state* has a core level electron and the photon. This is not altered by the neighboring atom.

X-ray absorption: Fermi's golden rule

$$\mu(E) = \mu_0(E)[1 + \chi(E)]$$

$$\chi(k[E]) = \frac{\mu(E) - \mu_0(E)}{\mu_0(E)}$$

$$k = \sqrt{\frac{2m(E - E_0)}{\hbar^2}}$$

$$\mu(E) \sim |\langle i|\mathcal{H}|f\rangle|^2$$

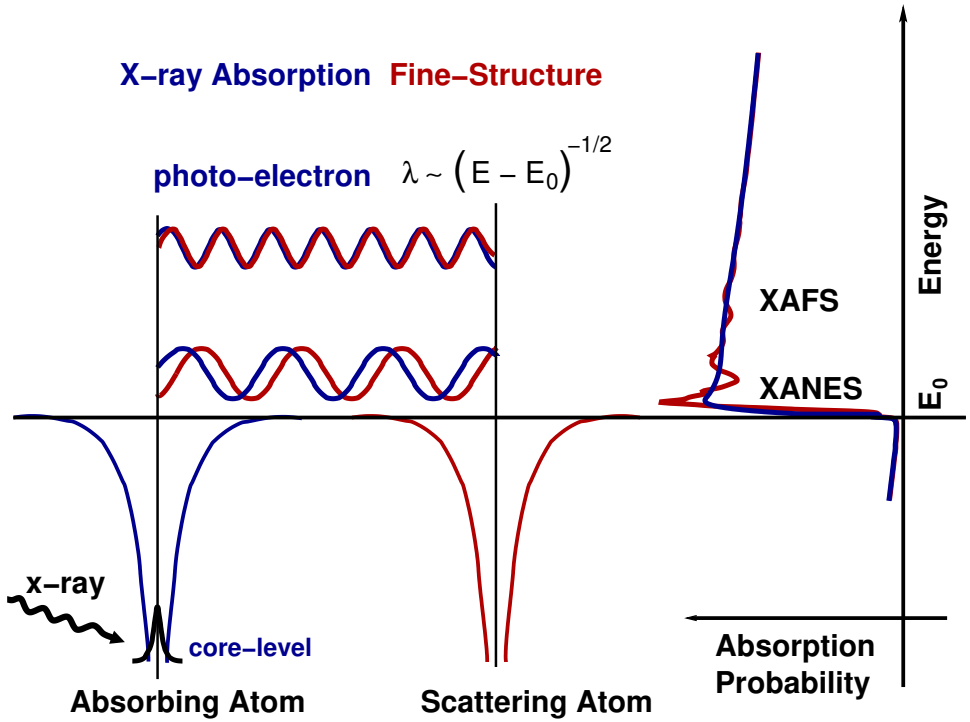

$\langle i|$ the *initial state* has a core level electron and the photon. This is not altered by the neighboring atom.

$\mathcal{H}$ the *interaction*. In the dipole approximation, $\mathcal{H} = e^{ikr} \approx 1$.

X-ray absorption: Fermi's golden rule

$$\mu(E) = \mu_0(E)[1 + \chi(E)]$$

$$\chi(k[E]) = \frac{\mu(E) - \mu_0(E)}{\mu_0(E)}$$

$$k = \sqrt{\frac{2m(E - E_0)}{\hbar^2}}$$

$$\mu(E) \sim |\langle i|\mathcal{H}|f\rangle|^2$$

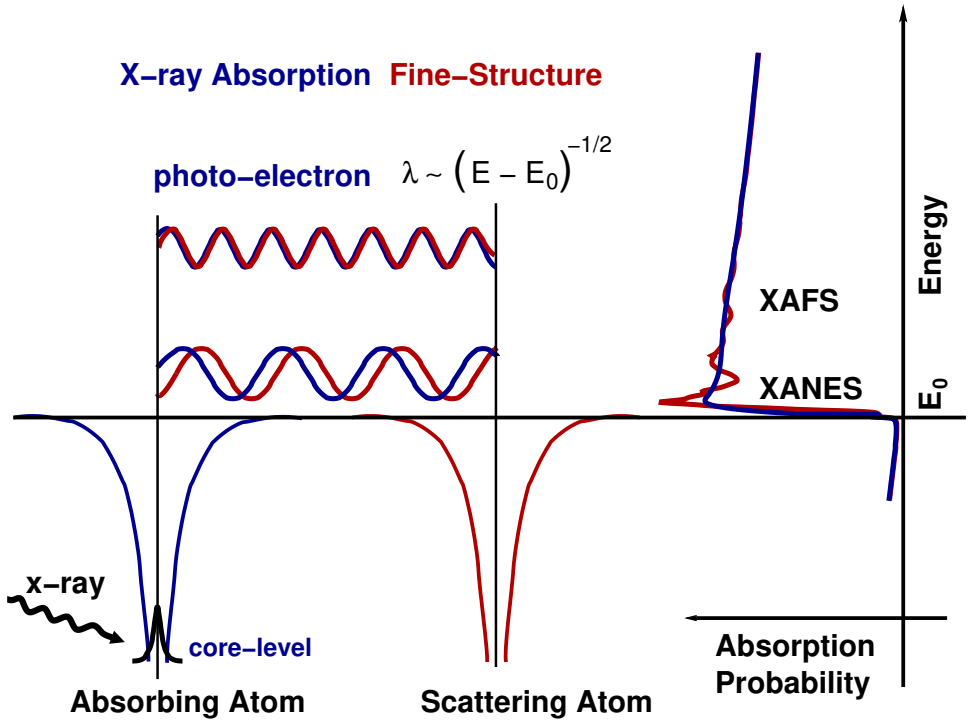

$\langle i|$ the *initial state* has a core level electron and the photon. This is not altered by the neighboring atom.

$\mathcal{H}$ the *interaction*. In the dipole approximation, $\mathcal{H} = e^{ikr} \approx 1$.

$|f\rangle$ the *final state* has a photo-electron, a hole in the core, and no photon. This is altered by the neighboring atom: the photo-electron scatters.

μ and χ and the photo-electron wavefunction

Writing $|f\rangle = |f_0 + \Delta f\rangle$, where Δf gives the change in photo-electron final state due to backscattering from the neighboring atom, we can expand μ to get

μ and χ and the photo-electron wavefunction

Writing $|f\rangle = |f_0 + \Delta f\rangle$, where Δf gives the change in photo-electron final state due to backscattering from the neighboring atom, we can expand μ to get

$$\mu(E) \sim |\langle i|\mathcal{H}|f_0\rangle|^2 \left[1 + \frac{\langle i|\mathcal{H}|\Delta f\rangle \langle f_0|\mathcal{H}|i\rangle^*}{|\langle i|\mathcal{H}|f_0\rangle|^2} + C.C.\right]$$

μ and χ and the photo-electron wavefunction

Writing $|f\rangle = |f_0 + \Delta f\rangle$, where Δf gives the change in photo-electron final state due to backscattering from the neighboring atom, we can expand μ to get

$$\mu(E) \sim |\langle i|\mathcal{H}|f_0\rangle|^2 \left[1 + \frac{\langle i|\mathcal{H}|\Delta f\rangle \langle f_0|\mathcal{H}|i\rangle^*}{|\langle i|\mathcal{H}|f_0\rangle|^2} + C.C.\right]$$

Compare this to $\mu(E) = \mu_0(E)[1 + \chi(E)]$ and we see

μ and χ and the photo-electron wavefunction

Writing $|f\rangle = |f_0 + \Delta f\rangle$, where Δf gives the change in photo-electron final state due to backscattering from the neighboring atom, we can expand μ to get

$$\mu(E) \sim |\langle i|\mathcal{H}|f_0\rangle|^2 \left[1 + \frac{\langle i|\mathcal{H}|\Delta f\rangle \langle f_0|\mathcal{H}|i\rangle^*}{|\langle i|\mathcal{H}|f_0\rangle|^2} + C.C.\right]$$

Compare this to $\mu(E) = \mu_0(E)[1 + \chi(E)]$ and we see

$$\begin{aligned} \mu_0(E) &\sim |\langle i|\mathcal{H}|f_0\rangle|^2 \\ \chi(E) &\sim \langle i|\mathcal{H}|\Delta f\rangle \sim \langle i|\Delta f\rangle \end{aligned}$$

μ and χ and the photo-electron wavefunction

Writing $|f\rangle = |f_0 + \Delta f\rangle$, where Δf gives the change in photo-electron final state due to backscattering from the neighboring atom, we can expand μ to get

$$\mu(E) \sim |\langle i|\mathcal{H}|f_0\rangle|^2 \left[1 + \frac{\langle i|\mathcal{H}|\Delta f\rangle \langle f_0|\mathcal{H}|i\rangle^*}{|\langle i|\mathcal{H}|f_0\rangle|^2} + C.C.\right]$$

Compare this to $\mu(E) = \mu_0(E)[1 + \chi(E)]$ and we see

$$\begin{aligned} \mu_0(E) &\sim & |\langle i|\mathcal{H}|f_0\rangle|^2 & \quad (\textit{atomic background}) \\ \chi(E) &\sim & \langle i|\mathcal{H}|\Delta f\rangle \sim \langle i|\Delta f\rangle & \quad (\textit{XAFS oscillations}) \end{aligned}$$

μ and χ and the photo-electron wavefunction

Writing $|f\rangle = |f_0 + \Delta f\rangle$, where Δf gives the change in photo-electron final state due to backscattering from the neighboring atom, we can expand μ to get

$$\mu(E) \sim |\langle i|\mathcal{H}|f_0\rangle|^2 \left[1 + \frac{\langle i|\mathcal{H}|\Delta f\rangle \langle f_0|\mathcal{H}|i\rangle^*}{|\langle i|\mathcal{H}|f_0\rangle|^2} + C.C.\right]$$

Compare this to $\mu(E) = \mu_0(E)[1 + \chi(E)]$ and we see

$$\begin{aligned} \mu_0(E) \sim & \quad |\langle i|\mathcal{H}|f_0\rangle|^2 & (\textit{atomic background}) \\ \chi(E) \sim & \quad \langle i|\mathcal{H}|\Delta f\rangle \sim \langle i|\Delta f\rangle & (\textit{XAFS oscillations}) \end{aligned}$$

Since the *initial state* – the core-level – is very nearly a delta-function in space, centered at the absorbing atom:

$$\chi \sim \langle i|\Delta f\rangle \sim \int dr \delta(r) \psi_{\mathrm{scatt}}(r) = \psi_{\mathrm{scatt}}(r = 0).$$

μ and χ and the photo-electron wavefunction

Writing $|f\rangle = |f_0 + \Delta f\rangle$, where Δf gives the change in photo-electron final state due to backscattering from the neighboring atom, we can expand μ to get

$$\mu(E) \sim |\langle i|\mathcal{H}|f_0\rangle|^2 \left[1 + \frac{\langle i|\mathcal{H}|\Delta f\rangle \langle f_0|\mathcal{H}|i\rangle^*}{|\langle i|\mathcal{H}|f_0\rangle|^2} + C.C.\right]$$

Compare this to $\mu(E) = \mu_0(E)[1 + \chi(E)]$ and we see

$$\begin{aligned} \mu_0(E) \sim & \quad |\langle i|\mathcal{H}|f_0\rangle|^2 & (\textit{atomic background}) \\ \chi(E) \sim & \quad \langle i|\mathcal{H}|\Delta f\rangle \sim \langle i|\Delta f\rangle & (\textit{XAFS oscillations}) \end{aligned}$$

Since the *initial state* – the core-level – is very nearly a delta-function in space, centered at the absorbing atom:

$$\chi \sim \langle i|\Delta f\rangle \sim \int dr \delta(r)\psi_{\rm scatt}(r) = \psi_{\rm scatt}(r=0).$$

χ is due to the portion of the photo-electron wave-function at the absorbing atom caused that was scattered back by neighboring atoms.

The EXAFS equation: simple description

With $\chi \sim \psi_{\mathrm{scatt}}(0)$, and a spherical wave for the photo-electron

$$\psi(k, r) = e^{ikr}/kr$$

we can model $\chi(k)$ as the photo-electron

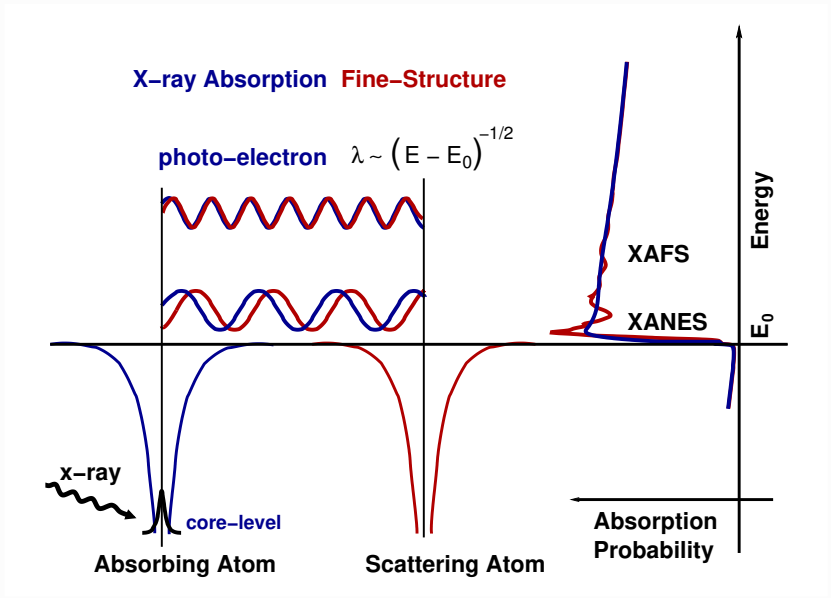

$$\chi(k) \sim \psi_{\mathrm{scatt}}(0)$$

The EXAFS equation: simple description

With $\chi \sim \psi_{\rm scatt}(0)$, and a spherical wave for the photo-electron

$$\psi(k,r) = e^{ikr}/kr$$

we can model $\chi(k)$ as the photo-electron

1. leaves the absorbing atom

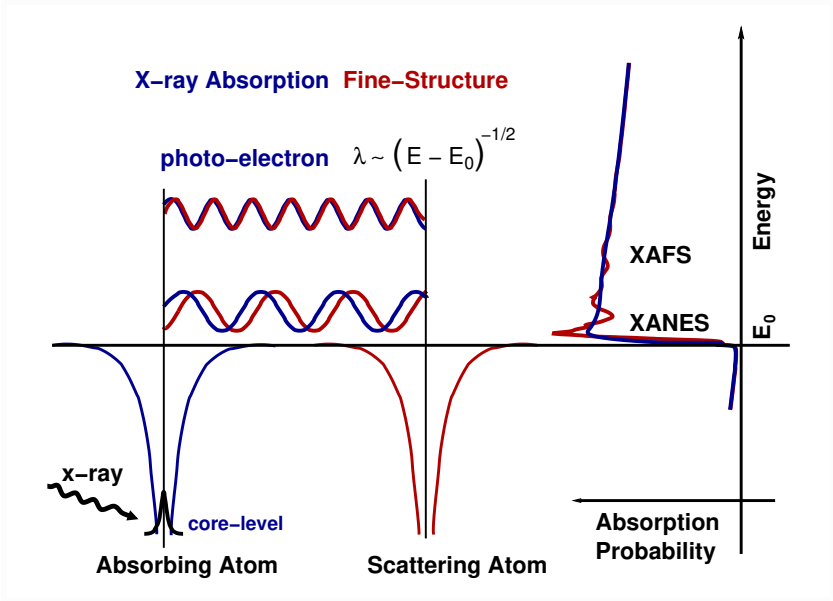

$$\chi(k) \sim \psi_{\rm scatt}(0) = \frac{e^{ikR}}{kR}$$

The EXAFS equation: simple description

With $\chi \sim \psi_{\rm scatt}(0)$, and a spherical wave for the photo-electron

$$\psi(k,r) = e^{ikr}/kr$$

we can model $\chi(k)$ as the photo-electron

1. leaves the absorbing atom
2. scatters from the neighbor atom

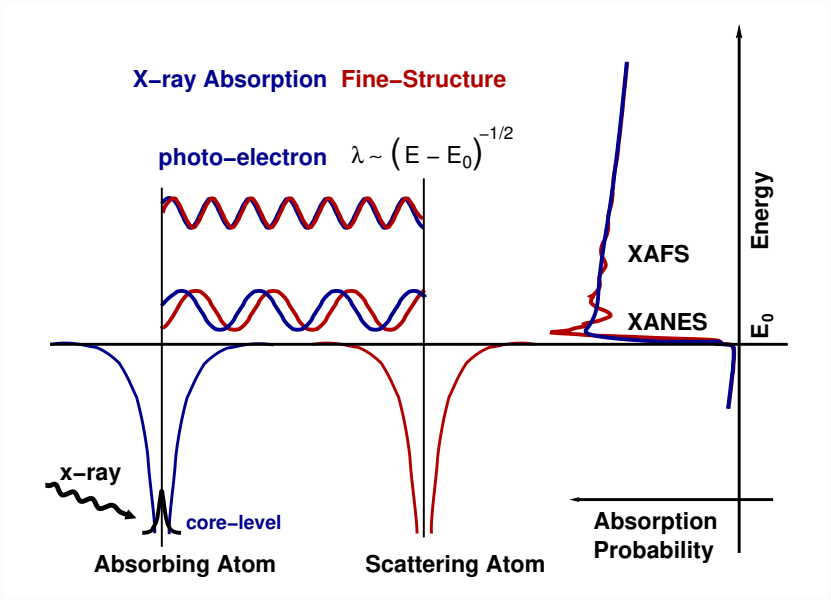

$$\chi(k) \sim \psi_{\rm scatt}(0) = \frac{e^{ikR}}{kR}\,[2kf(k)e^{i\delta(k)}]$$

where scattering from the neighboring atom gives the amplitude $f(k)$ and phase-shift $\delta(k)$ to the photo-electron.

The EXAFS equation: simple description

With $\chi \sim \psi_{\rm scatt}(0)$, and a spherical wave for the photo-electron

$$\psi(k,r) = e^{ikr}/kr$$

we can model $\chi(k)$ as the photo-electron

1. leaves the absorbing atom
2. scatters from the neighbor atom
3. returns to the absorbing atom

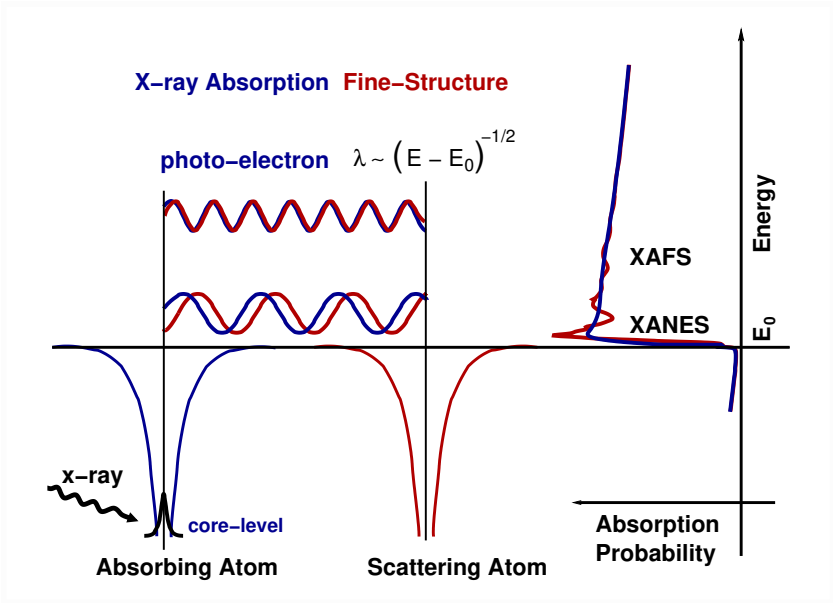

$$\chi(k) \sim \psi_{\rm scatt}(0) = \frac{e^{ikR}}{kR}\left[2kf(k)e^{i\delta(k)}\right]\frac{e^{ikR}}{kR}$$

where scattering from the neighboring atom gives the amplitude $f(k)$ and phase-shift $\delta(k)$ to the photo-electron.

The EXAFS equation: simple description

With $\chi \sim \psi_{\rm scatt}(0)$, and a spherical wave for the photo-electron

$$\psi(k,r) = e^{ikr}/kr$$

we can model $\chi(k)$ as the photo-electron

1. leaves the absorbing atom
2. scatters from the neighbor atom
3. returns to the absorbing atom

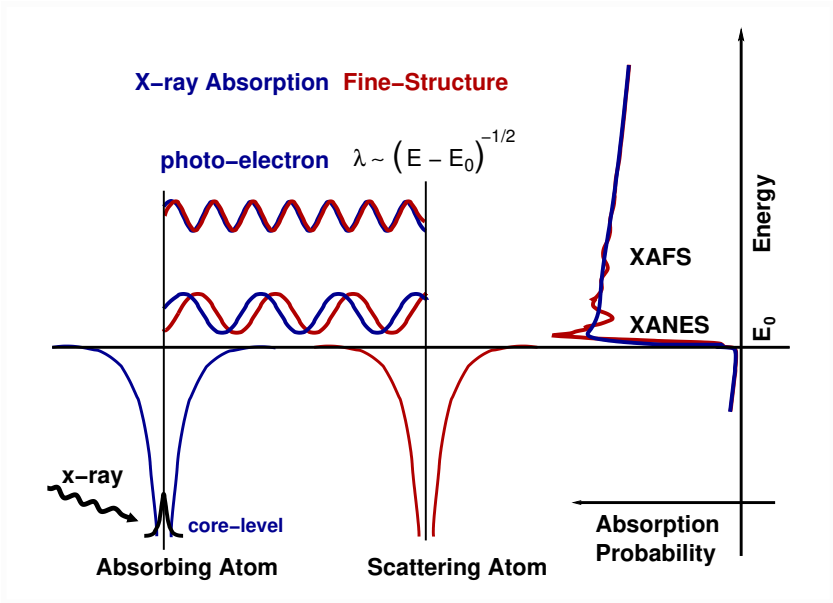

$$\chi(k) \sim \psi_{\rm scatt}(0) = \frac{e^{ikR}}{kR}\left[2kf(k)e^{i\delta(k)}\right]\frac{e^{ikR}}{kR} + C.C.$$

where scattering from the neighboring atom gives the amplitude $f(k)$ and phase-shift $\delta(k)$ to the photo-electron.

Development of the EXAFS equation

Including the complex conjugate, and insisting on a Real value, we get

$$\chi(k) = \frac{f(k)}{kR^2}\sin[2kR + \delta(k)]$$

Development of the EXAFS equation

Including the complex conjugate, and insisting on a Real value, we get

$$\chi(k) = \frac{f(k)}{kR^2}\sin[2kR + \delta(k)]$$

The EXAFS Equation for 1 scattering atom.

Development of the EXAFS equation

Including the complex conjugate, and insisting on a Real value, we get

$$\chi(k) = \frac{f(k)}{kR^2}\sin[2kR + \delta(k)]$$

The EXAFS Equation for 1 scattering atom.

For N neighboring atoms, and with thermal and static disorder of σ^2, giving the *mean-square disorder* in R, we have

$$\chi(k) = \frac{Nf(k)e^{-2k^2\sigma^2}}{kR^2}\sin\left[2kR + \delta(k)\right]$$

Development of the EXAFS equation

Including the complex conjugate, and insisting on a Real value, we get

$$\chi(k) = \frac{f(k)}{kR^2}\sin[2kR + \delta(k)]$$

The EXAFS Equation for 1 scattering atom.

For N neighboring atoms, and with thermal and static disorder of σ^2, giving the *mean-square disorder* in R, we have

$$\chi(k) = \frac{Nf(k)e^{-2k^2\sigma^2}}{kR^2}\sin\left[2kR + \delta(k)\right]$$

A real system has atoms at different distances and of different types. We add all these contributions to get a better version of the EXAFS equation:

$$\chi(k) = \sum_j \frac{N_j f_j(k) e^{-2k^2\sigma_j^2}}{kR_j^2}\sin[2kR_j + \delta_j(k)]$$

Scattering amplitude and phase shift: $f(k)$ and $\delta(k)$

The scattering amplitude $f(k)$ and phase-shift $\delta(k)$ depend on atomic number.

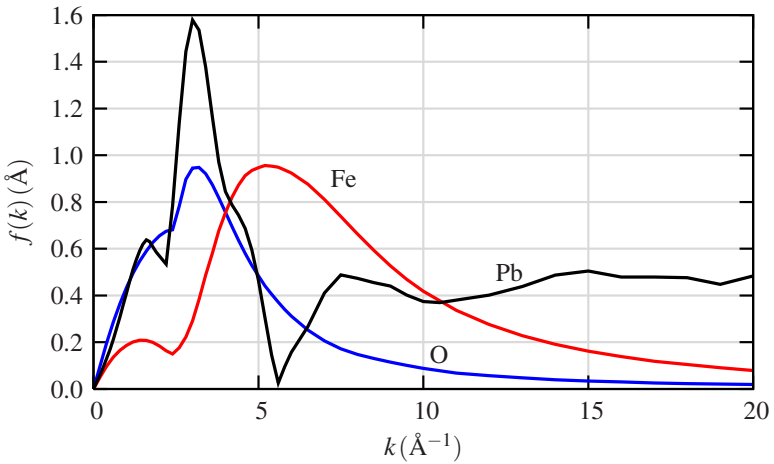

The scattering amplitude $f(k)$ peaks at different k values and extends to higher-k for heavier elements. For very heavy elements, there is structure in $f(k)$.

Scattering amplitude and phase shift: $f(k)$ and $\delta(k)$

The scattering amplitude $f(k)$ and phase-shift $\delta(k)$ depend on atomic number.

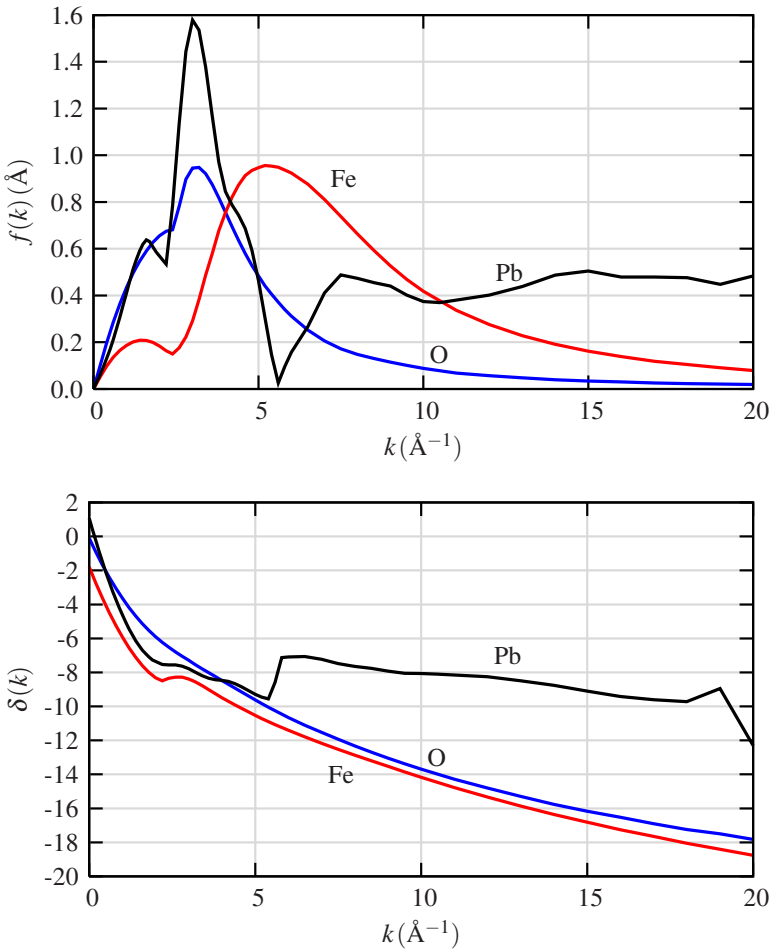

The scattering amplitude $f(k)$ peaks at different k values and extends to higher-k for heavier elements. For very heavy elements, there is structure in $f(k)$.

The phase shift $\delta(k)$ shows sharp changes for very heavy elements.

Z can usually be determined to ± 5. Fe and O can be distinguished, but Fe and Mn cannot be.

The EXAFS equation

The full EXAFS calculation includes mean free path $\lambda(k)$ and amplitude reduction factor S_0^2. The oscillations can be modelled and interpreted using a conceptually simple method (the details are subtle!):

The EXAFS equation

The full EXAFS calculation includes mean free path $\lambda(k)$ and amplitude reduction factor S_0^2. The oscillations can be modelled and interpreted using a conceptually simple method (the details are subtle!):

$$\chi(k) = \sum_j \frac{N_j S_0^2 f_j(k) e^{-2R_j/\lambda(k)} e^{-2k^2\sigma_j^2}}{k{R_j}^2} \sin\left[2kR_j + \delta_j(k)\right]$$

The EXAFS equation

The full EXAFS calculation includes mean free path $\lambda(k)$ and amplitude reduction factor S_0^2. The oscillations can be modelled and interpreted using a conceptually simple method (the details are subtle!):

$$\chi(k) = \sum_j \frac{N_j S_0^2 f_j(k) e^{-2R_j/\lambda(k)} e^{-2k^2\sigma_j^2}}{k {R_j}^2} \sin\left[2kR_j + \delta_j(k)\right]$$

where the sum could be over shells of atoms (Fe-O, Fe-Fe) or ...

The EXAFS equation

The full EXAFS calculation includes mean free path $\lambda(k)$ and amplitude reduction factor S_0^2. The oscillations can be modelled and interpreted using a conceptually simple method (the details are subtle!):

$$\chi(k) = \sum_j \frac{N_j S_0^2 f_j(k) e^{-2R_j/\lambda(k)} e^{-2k^2\sigma_j^2}}{k {R_j}^2} \sin\left[2kR_j + \delta_j(k)\right]$$

where the sum could be over shells of atoms (Fe-O, Fe-Fe) or . . .
. . . over scattering paths for the photo-electron.

The EXAFS equation

The full EXAFS calculation includes mean free path $\lambda(k)$ and amplitude reduction factor S_0^2. The oscillations can be modelled and interpreted using a conceptually simple method (the details are subtle!):

$$\chi(k) = \sum_j \frac{N_j S_0^2 f_j(k) e^{-2R_j/\lambda(k)} e^{-2k^2\sigma_j^2}}{k R_j^2} \sin\left[2kR_j + \delta_j(k)\right]$$

where the sum could be over shells of atoms (Fe-O, Fe-Fe) or . . .
. . . over scattering paths for the photo-electron.

N_j: path degeneracy

The EXAFS equation

The full EXAFS calculation includes mean free path $\lambda(k)$ and amplitude reduction factor S_0^2. The oscillations can be modelled and interpreted using a conceptually simple method (the details are subtle!):

$$\chi(k) = \sum_j \frac{N_j S_0^2 f_j(k) e^{-2R_j/\lambda(k)} e^{-2k^2\sigma_j^2}}{kR_j^2} \sin\left[2kR_j + \delta_j(k)\right]$$

where the sum could be over shells of atoms (Fe-O, Fe-Fe) or . . .
. . . over scattering paths for the photo-electron.

N_j: path degeneracy

R_j: half path length

The EXAFS equation

The full EXAFS calculation includes mean free path $\lambda(k)$ and amplitude reduction factor S_0^2. The oscillations can be modelled and interpreted using a conceptually simple method (the details are subtle!):

$$\chi(k) = \sum_j \frac{N_j S_0^2 f_j(k) e^{-2R_j/\lambda(k)} e^{-2k^2\sigma_j^2}}{kR_j^2} \sin\left[2kR_j + \delta_j(k)\right]$$

where the sum could be over shells of atoms (Fe-O, Fe-Fe) or . . .
. . . over scattering paths for the photo-electron.

N_j: path degeneracy

R_j: half path length

σ_j^2: path "disorder"

The EXAFS equation

The full EXAFS calculation includes mean free path $\lambda(k)$ and amplitude reduction factor S_0^2. The oscillations can be modelled and interpreted using a conceptually simple method (the details are subtle!):

$$\chi(k) = \sum_j \frac{N_j S_0^2 f_j(k) e^{-2R_j/\lambda(k)}\, e^{-2k^2\sigma_j^2}}{kR_j^2} \sin\left[2kR_j + \delta_j(k)\right]$$

where the sum could be over shells of atoms (Fe-O, Fe-Fe) or . . .
. . . over scattering paths for the photo-electron.

- N_j: path degeneracy
- R_j: half path length
- σ_j^2: path "disorder"
- S_0^2: amplitude reduction factor

The EXAFS equation

The full EXAFS calculation includes mean free path $\lambda(k)$ and amplitude reduction factor S_0^2. The oscillations can be modelled and interpreted using a conceptually simple method (the details are subtle!):

$$\chi(k) = \sum_j \frac{N_j S_0^2 f_j(k) e^{-2R_j/\lambda(k)} e^{-2k^2\sigma_j^2}}{k {R_j}^2} \sin\left[2kR_j + \delta_j(k)\right]$$

where the sum could be over shells of atoms (Fe-O, Fe-Fe) or . . .
. . . over scattering paths for the photo-electron.

N_j: path degeneracy

R_j: half path length

σ_j^2: path "disorder"

S_0^2: amplitude reduction factor

k is the photoelectron wave number

The EXAFS equation

The full EXAFS calculation includes mean free path $\lambda(k)$ and amplitude reduction factor S_0^2. The oscillations can be modelled and interpreted using a conceptually simple method (the details are subtle!):

$$\chi(k) = \sum_j \frac{N_j S_0^2 f_j(k) e^{-2R_j/\lambda(k)} e^{-2k^2\sigma_j^2}}{kR_j^2} \sin\left[2kR_j + \delta_j(k)\right]$$

where the sum could be over shells of atoms (Fe-O, Fe-Fe) or . . .
. . . over scattering paths for the photo-electron.

- N_j: path degeneracy
- R_j: half path length
- σ_j^2: path "disorder"
- S_0^2: amplitude reduction factor

k is the photoelectron wave number

$f_j(k)$: scattering factor for the path

The EXAFS equation

The full EXAFS calculation includes mean free path $\lambda(k)$ and amplitude reduction factor S_0^2. The oscillations can be modelled and interpreted using a conceptually simple method (the details are subtle!):

$$\chi(k) = \sum_j \frac{N_j S_0^2 f_j(k) e^{-2R_j/\lambda(k)} e^{-2k^2\sigma_j^2}}{kR_j^2} \sin\left[2kR_j + \delta_j(k)\right]$$

where the sum could be over shells of atoms (Fe-O, Fe-Fe) or . . .
. . . over scattering paths for the photo-electron.

- N_j: path degeneracy
- R_j: half path length
- σ_j^2: path "disorder"
- S_0^2: amplitude reduction factor

k is the photoelectron wave number

- $f_j(k)$: scattering factor for the path
- $\delta_j(k)$: phase shift for the path

The EXAFS equation

The full EXAFS calculation includes mean free path $\lambda(k)$ and amplitude reduction factor S_0^2. The oscillations can be modelled and interpreted using a conceptually simple method (the details are subtle!):

$$\chi(k) = \sum_j \frac{N_j S_0^2 f_j(k) e^{-2R_j/\lambda(k)} e^{-2k^2\sigma_j^2}}{kR_j^2} \sin\left[2kR_j + \delta_j(k)\right]$$

where the sum could be over shells of atoms (Fe-O, Fe-Fe) or . . .
. . . over scattering paths for the photo-electron.

- N_j: path degeneracy
- R_j: half path length
- σ_j^2: path "disorder"
- S_0^2: amplitude reduction factor
- k is the photoelectron wave number
- $f_j(k)$: scattering factor for the path
- $\delta_j(k)$: phase shift for the path
- $\lambda(k)$: photoelectron mean free path

The EXAFS equation

The full EXAFS calculation includes mean free path $\lambda(k)$ and amplitude reduction factor S_0^2. The oscillations can be modelled and interpreted using a conceptually simple method (the details are subtle!):

$$\chi(k) = \sum_j \frac{N_j S_0^2 f_j(k) e^{-2R_j/\lambda(k)} e^{-2k^2\sigma_j^2}}{kR_j^2} \sin\left[2kR_j + \delta_j(k)\right]$$

where the sum could be over shells of atoms (Fe-O, Fe-Fe) or ...
...over scattering paths for the photo-electron.

- N_j: path degeneracy
- R_j: half path length
- σ_j^2: path "disorder"
- S_0^2: amplitude reduction factor
- k is the photoelectron wave number
- $f_j(k)$: scattering factor for the path
- $\delta_j(k)$: phase shift for the path
- $\lambda(k)$: photoelectron mean free path

Because we can compute $f(k)$ and $\delta(k)$, and $\lambda(k)$ we can determine Z, R, N, and σ^2 for scattering paths to neighboring atoms by fitting the data.

Advantages of nanoferritic alloy (NFA) steels

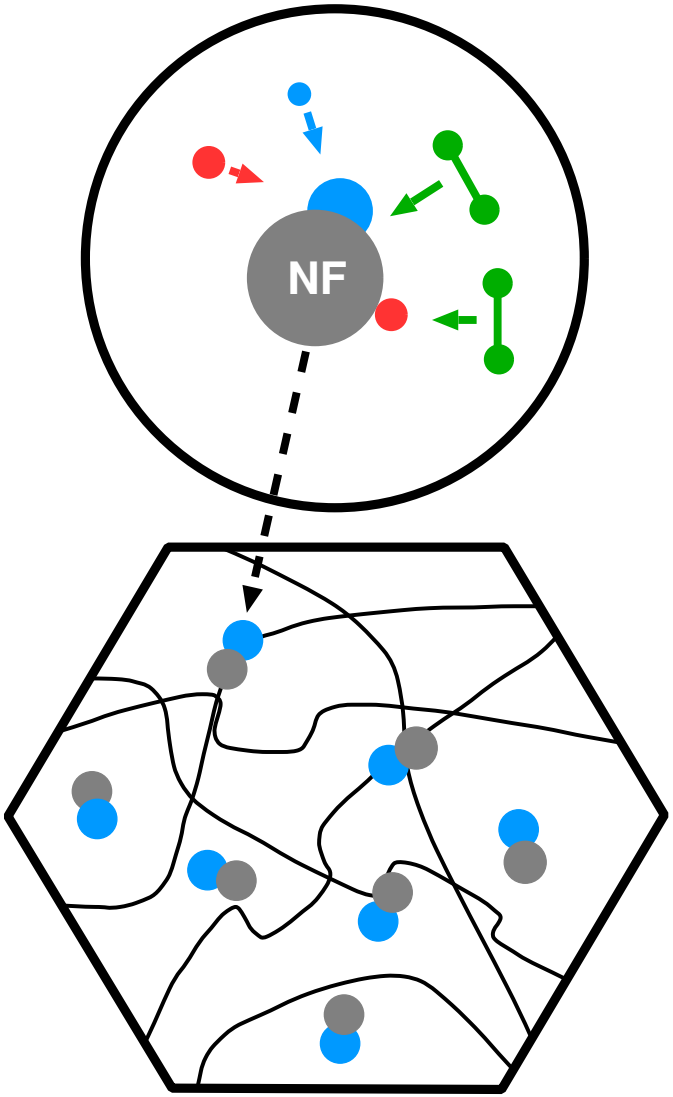

High density nanofeatures (NFs) and dislocations provide irradiation damage resistance

NFs trap helium in fine bubbles and prevent accumulation of high concentrations

NFs maintain high stable sink densities for vacancy and self-interstitial atom defect annihilation

NFs maintain high creep strength because of dislocation pinning, allowing operation at temperatures above the displacement damage regime

G.R. Odette, M.J. Alinger, and B.D. Wirth, *Annu. Rev. Mater. Res.* **38**, 471–503 (2008).

Fabrication of NFA steels

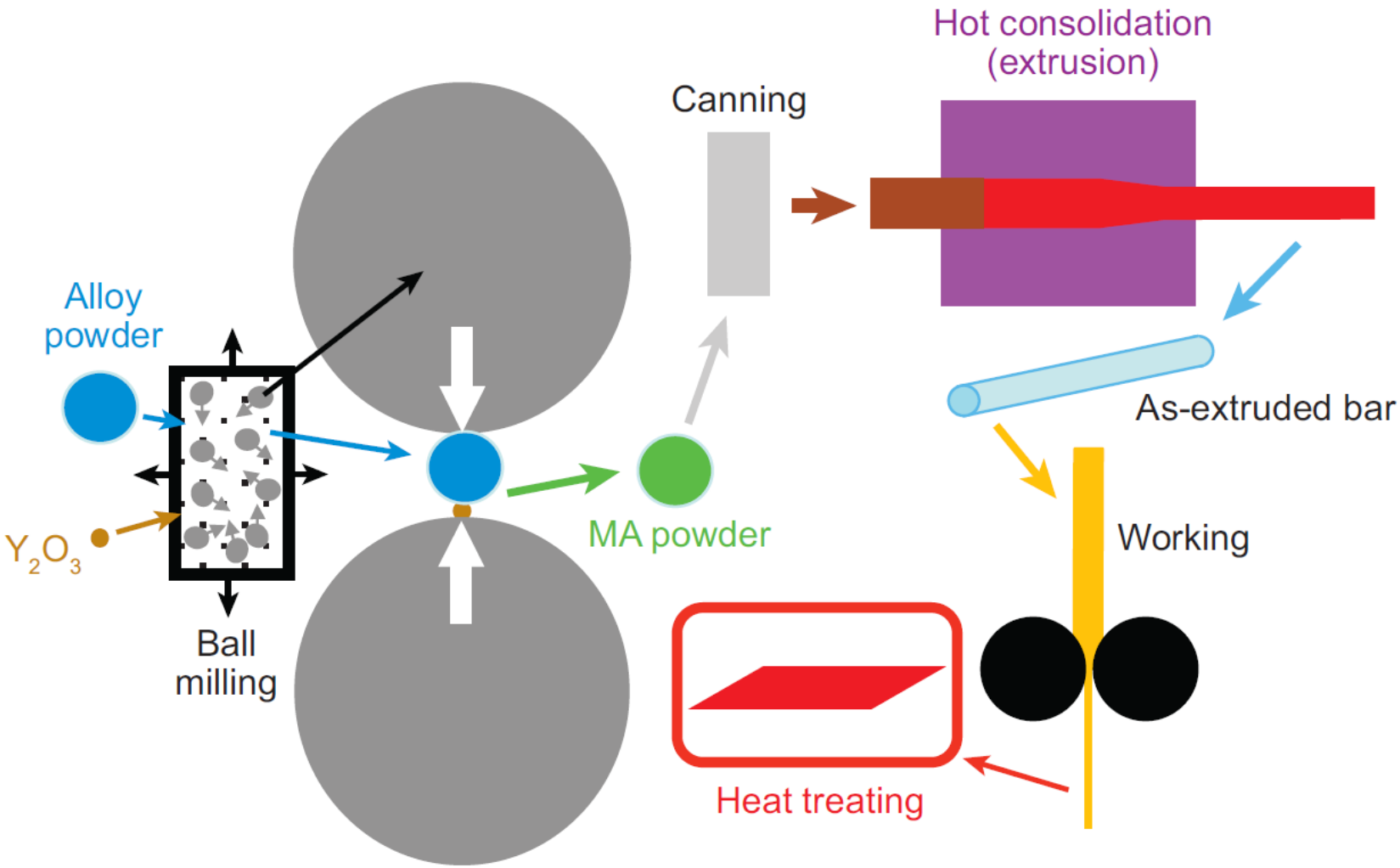

G.R. Odette, M.J. Alinger, and B.D.Wirth, *Annu. Rev. Mater. Res.* **38**, 471–503 (2008).

Atom probe tomography data

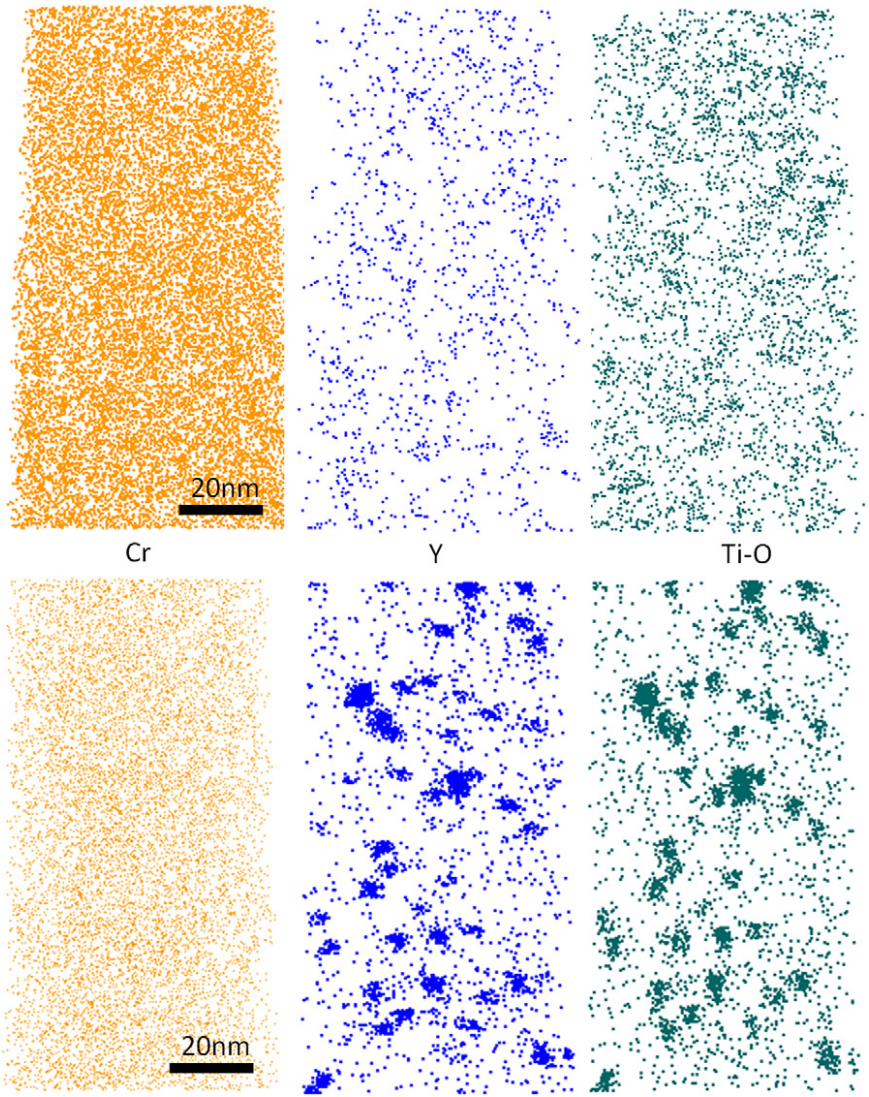

After mechanical alloying, Cr, Ti and Y are uniformly distributed throughout the solid

Consolidated materials show Ti-O and Y to be primarily co-localized in nanoclusters

Use XAS to understand the local structure of these nanoclusters

C.A. Williams, P. Unifantowicz, N. Baluc, G.D.W. Smith, and E.A. Marquis, *Acta Materialia* **61**, 2219–2235 (2013).

Samples studied

Sample name	Composition (wt %)					Processing
	Cr	Ti	Mo	W	Y_2O_3	
MA957	14	1	0.3		0.3	hot extruded @ 1150°C
J12YWT	12	0.4		3	0.25	hot extruded @ 1150°C
as received	14	0.4		3		as received powder
as milled	14	0.4		3	0.25	mechanically alloyed powder
850°C	14	0.4		3	0.25	powder annealed @ 850°C
1000°C	14	0.4		3	0.25	powder annealed @ 1000°C
1150°C	14	0.4		3	0.25	powder annealed @ 1150°C

Samples consolidated from as milled powder by hot isostatic pressing were shown to be identical to annealed powders and are thus not discussed.

Yttrium edge data

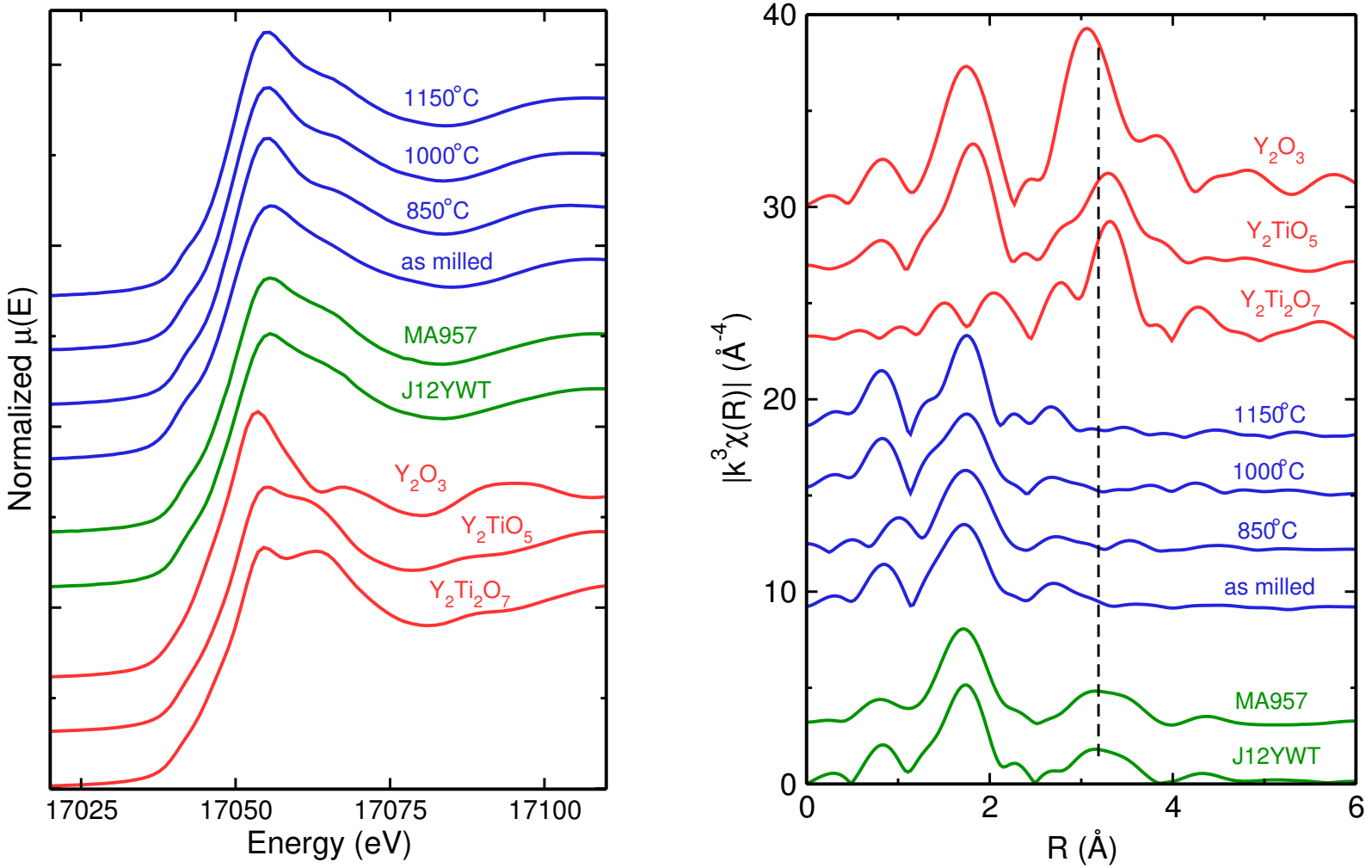

Edges show complex mixture; EXAFS of annealed powders indicate smaller NFs than commercial steels

Titanium edge data

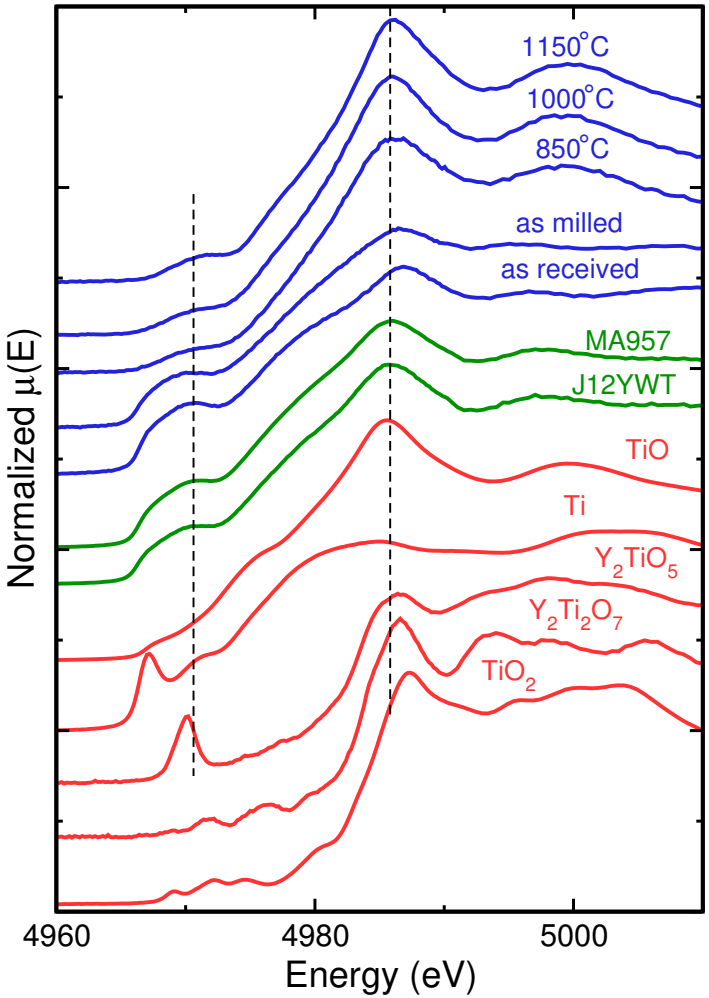

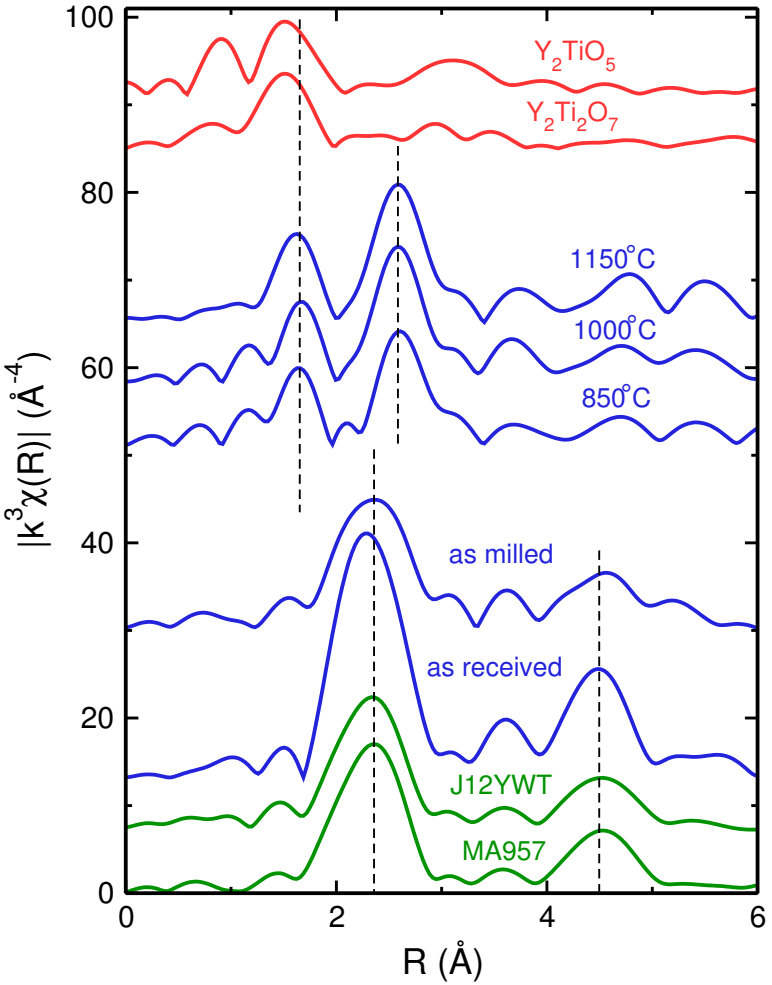

As received, as milled and commercial steels all show a metallic environment; annealed powder edges resemble TiO and EXAFS shows a distinct heavy metal peak at ~ 2.6Å

Ti in BCC structure

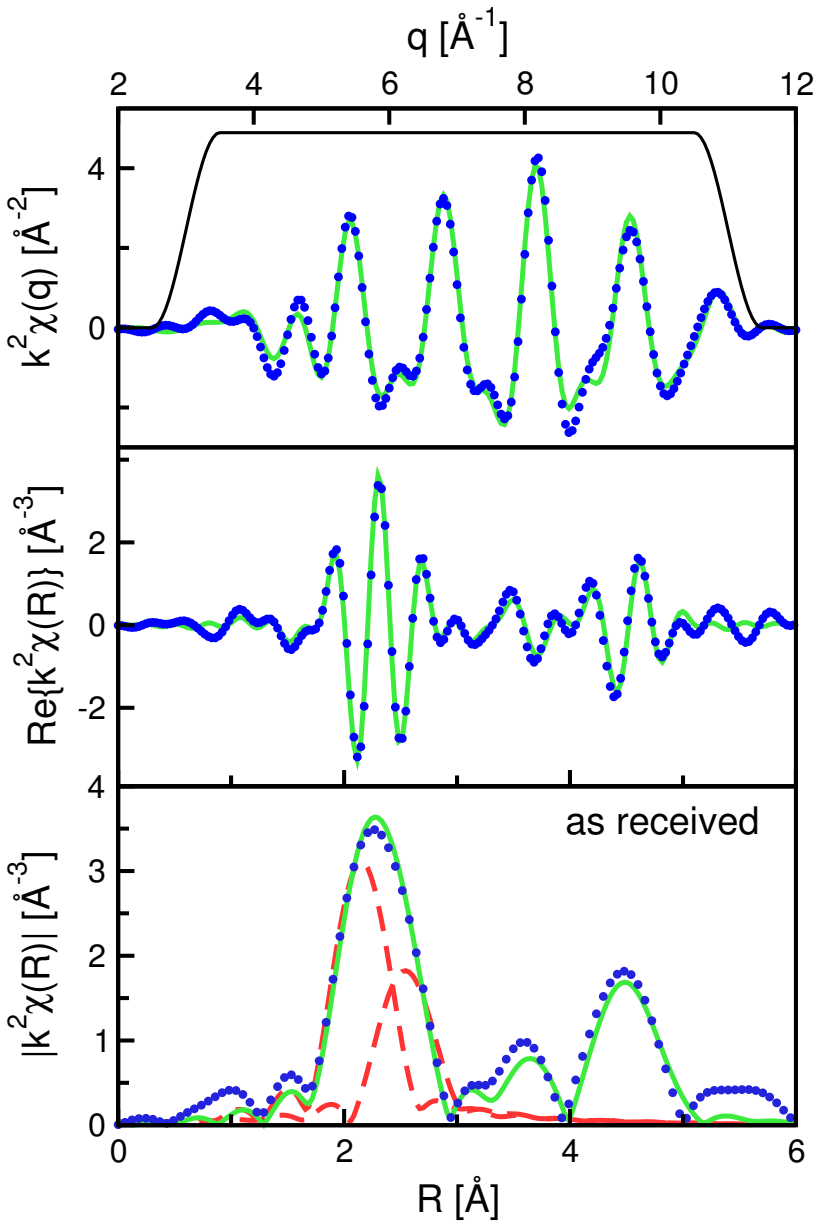

As received data can be fit with a simple BCC Fe model

Ti in BCC structure

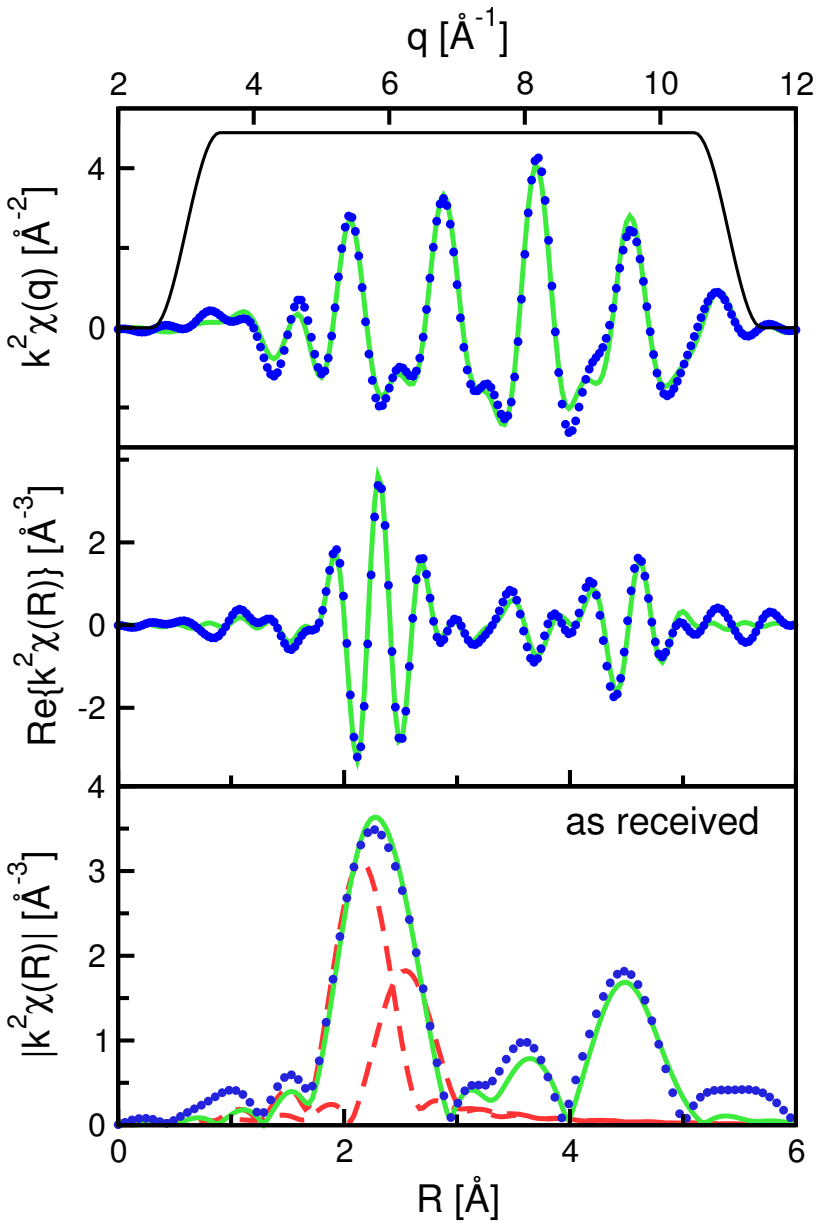

As received data can be fit with a simple BCC Fe model

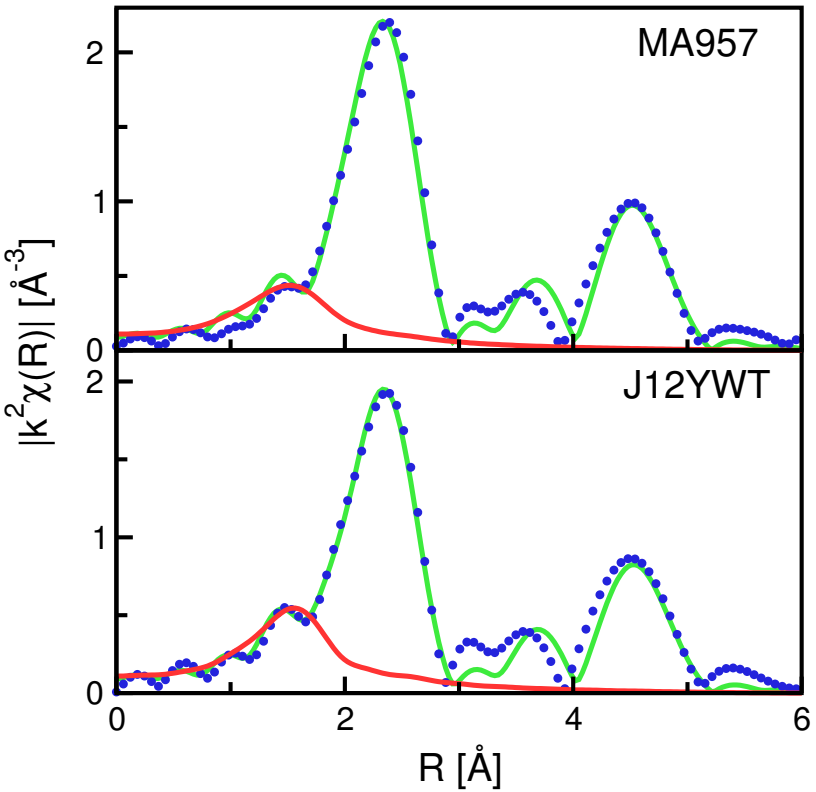

Commercial alloys fit with this model plus a small amount of Ti-O neighbors

Ti in TiO structure

Annealed powders have a remarkable resemblance to the cubic TiO calculated spectrum

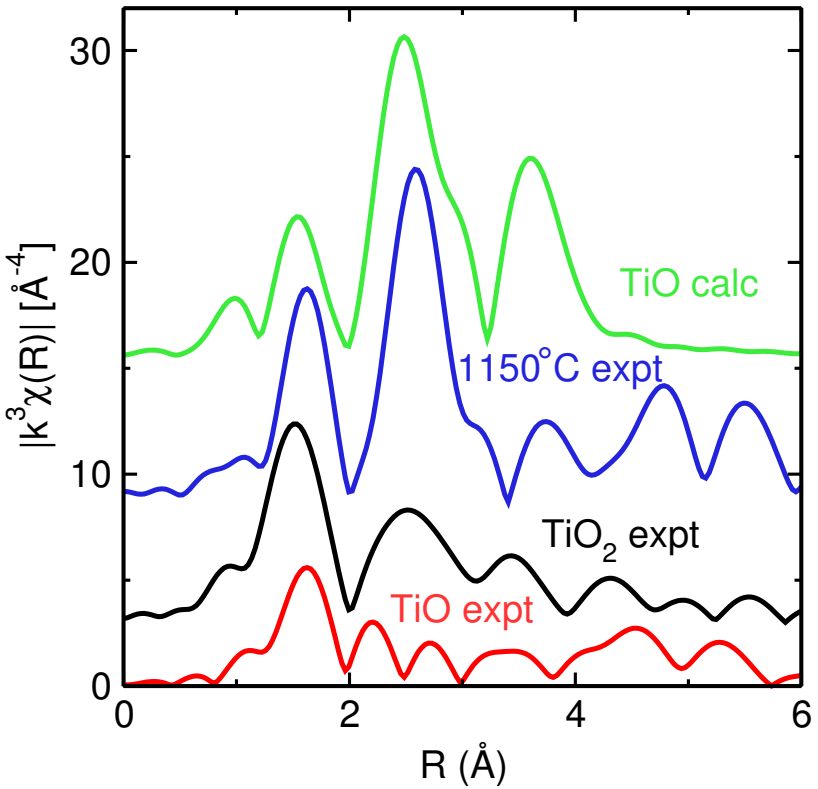

Ti in TiO structure

Annealed powders have a remarkable resemblance to the cubic TiO calculated spectrum

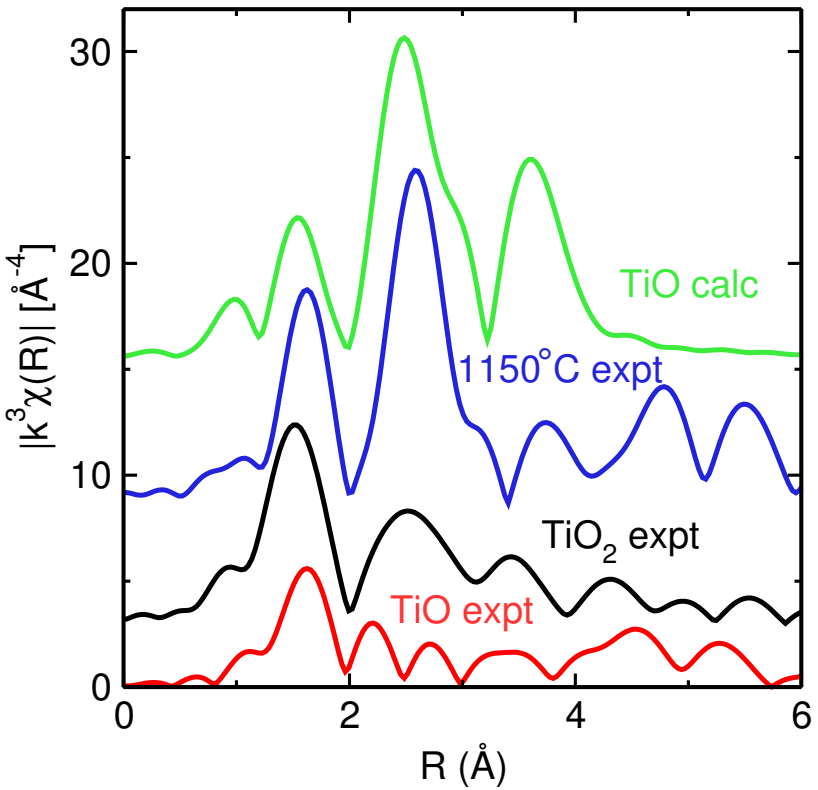

All can be fit with cubic TiO plus an additional Ti–O path, likely from complex Y–Ti–O oxides

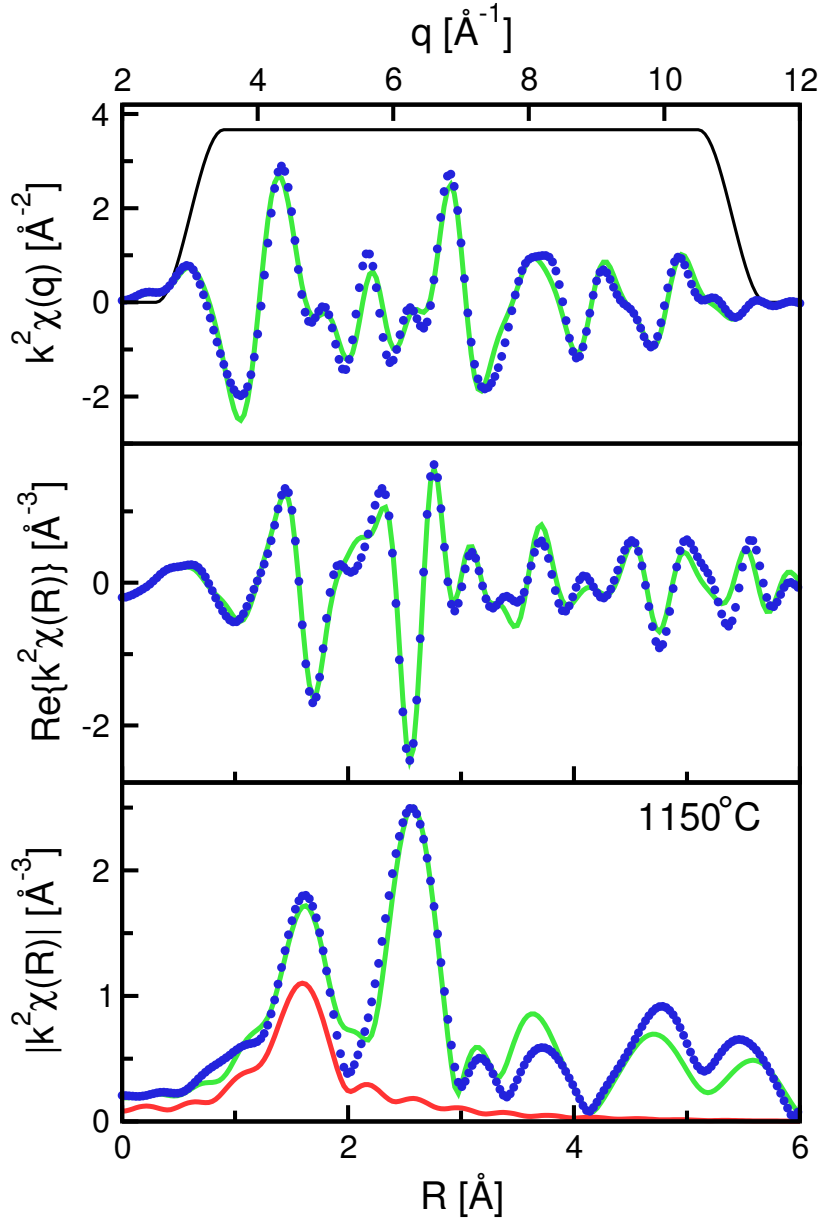

The fate of Ti

Commercial steels retain Ti in a metallic BCC lattice for the most part

Annealed powders all have mixture of TiO-like structure and more complex oxides ($\sim$ 50% each)

Presence of this metastable cubic TiO suggests significant fraction of Ti on the surface of Y–Ti–O NFs (consistent with Marquis & Williams)

The fate of Ti

Commercial steels retain Ti in a metallic BCC lattice for the most part

Annealed powders all have mixture of TiO-like structure and more complex oxides ($\sim$ 50% each)

Presence of this metastable cubic TiO suggests significant fraction of Ti on the surface of Y–Ti–O NFs (consistent with Marquis & Williams)

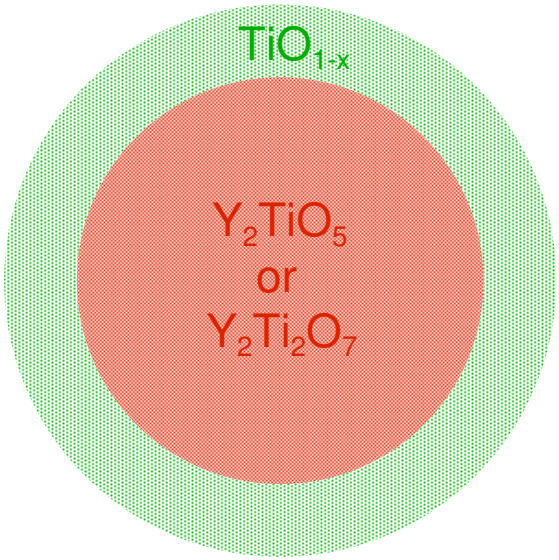

TiO cubic suboxide is stabilized on the surface of the Y–Ti–O nanoclusters

The fate of Ti

Commercial steels retain Ti in a metallic BCC lattice for the most part

Annealed powders all have mixture of TiO-like structure and more complex oxides ($\sim$ 50% each)

Presence of this metastable cubic TiO suggests significant fraction of Ti on the surface of Y–Ti–O NFs (consistent with Marquis & Williams)

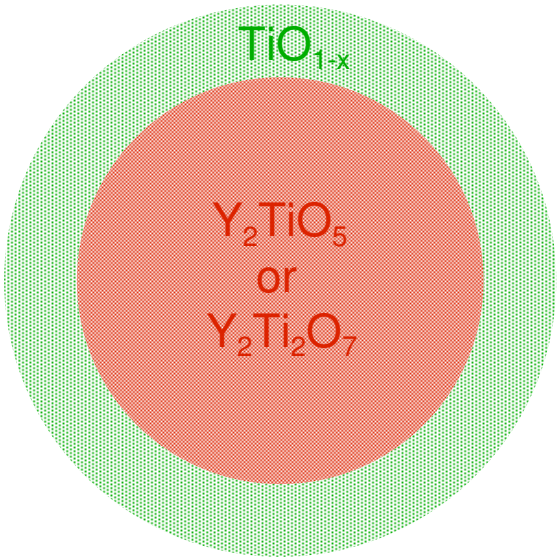

TiO cubic suboxide is stabilized on the surface of the Y–Ti–O nanoclusters

S. Liu, G.R. Odette, and C.U. Segre, *J. Nucl. Mater.* **445**, 50-56 (2014).

Mark I operando fuel cell

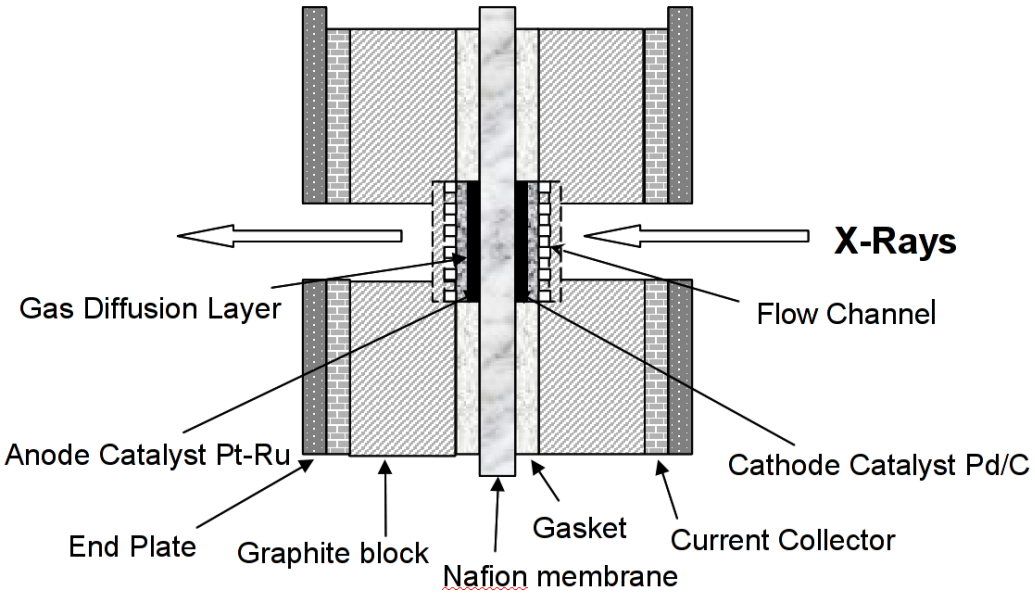

- Transmission mode
- <1 mm of graphite
- Pt/Ru on anode
- Pd on cathode
- 35°C operating temp
- 1-2 min scan time

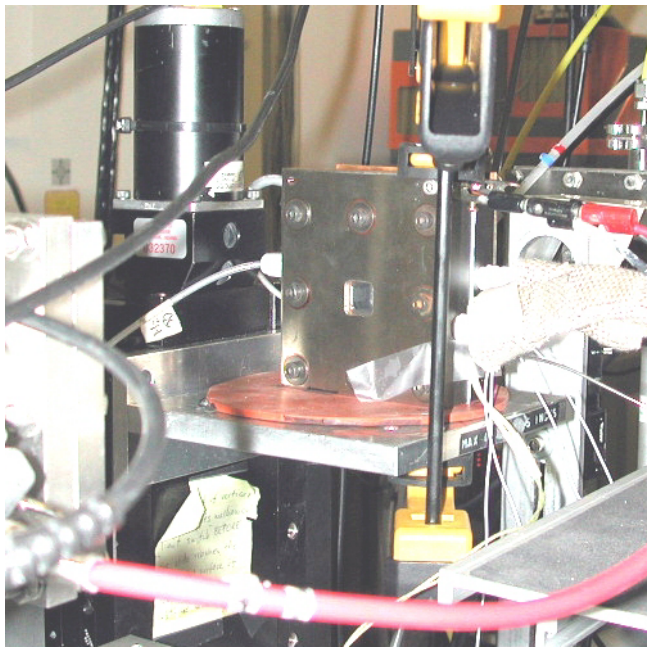

R. Viswanathan et al., "In-situ XANES study of carbon supported Pt-Ru anode electrocatalysts for reformate-air polymer electrolyte fuel cells", *J. Phys. Chem.* **B 106**, 3458 (2002).

Mark II operando fuel cell

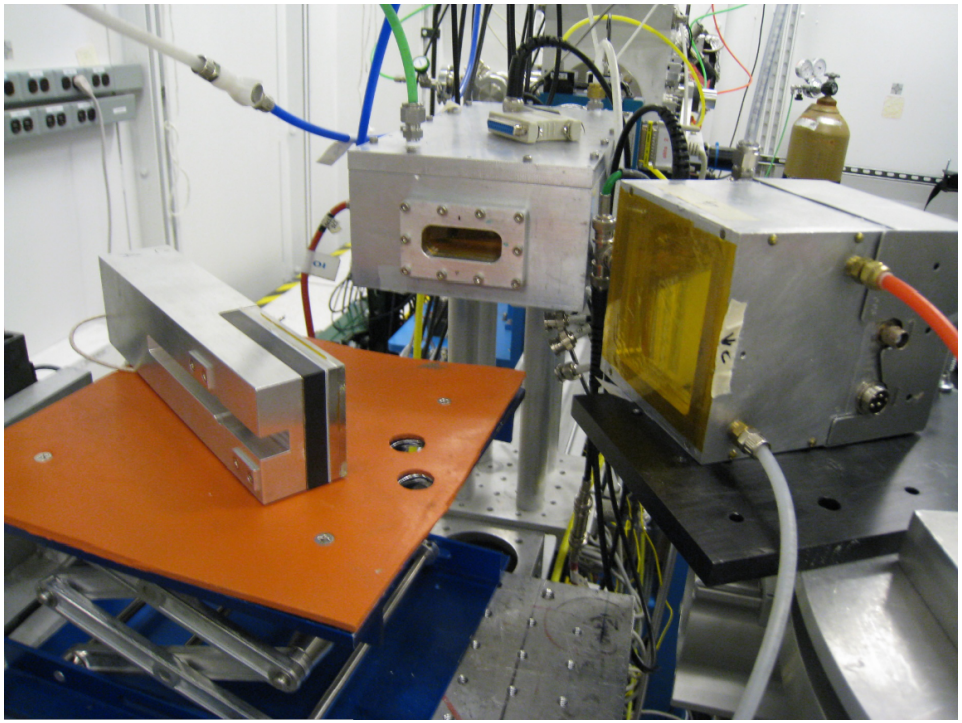

- Air-breathing cathode
- Pd on anode
- 1.2 mg/cm^2 loading
- 50°C operating temp
- Pt L_3 and Ni K edges
- Continuous scan mode @

mrcat

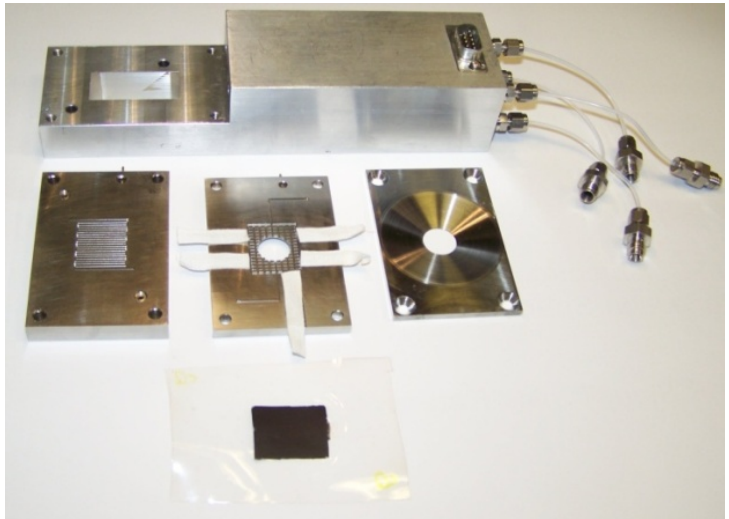

E.A. Lewis et al., "Operando x-ray absorption and infrared fuel cell spectroscopy", *Electrochim. Acta.* **56**, 8827 (2011).

Oxygen reduction at a PtNi cathode

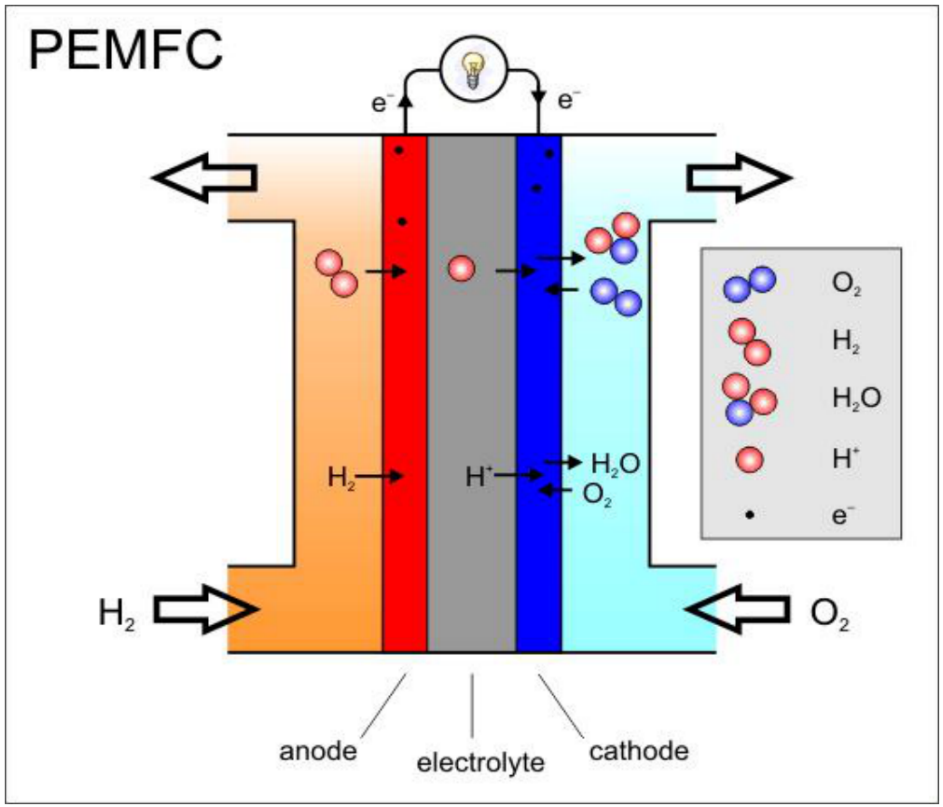

U.S. Department of Defense (DoD) Fuel Cell Test and Evaluation Center (FCTec)

Anode: 0 V vs. SHE

$$2\,H_2 \longrightarrow 4\,H^+ + 4\,e^-$$

Cathode: 1.23 V s. SHE

$$O_2 + 4\,H^+ + 4\,e^- \longrightarrow 2\,H_2O$$

breaking O−O bond is the rate limiting step

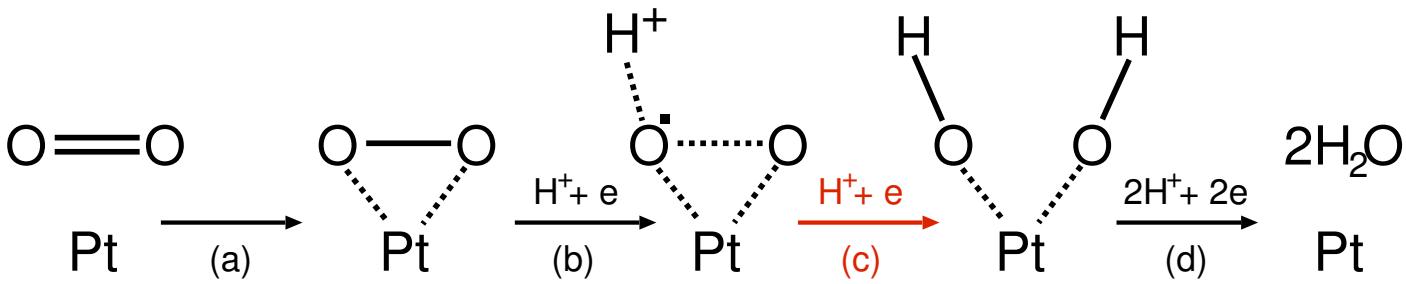

Fuel cell performance and open questions

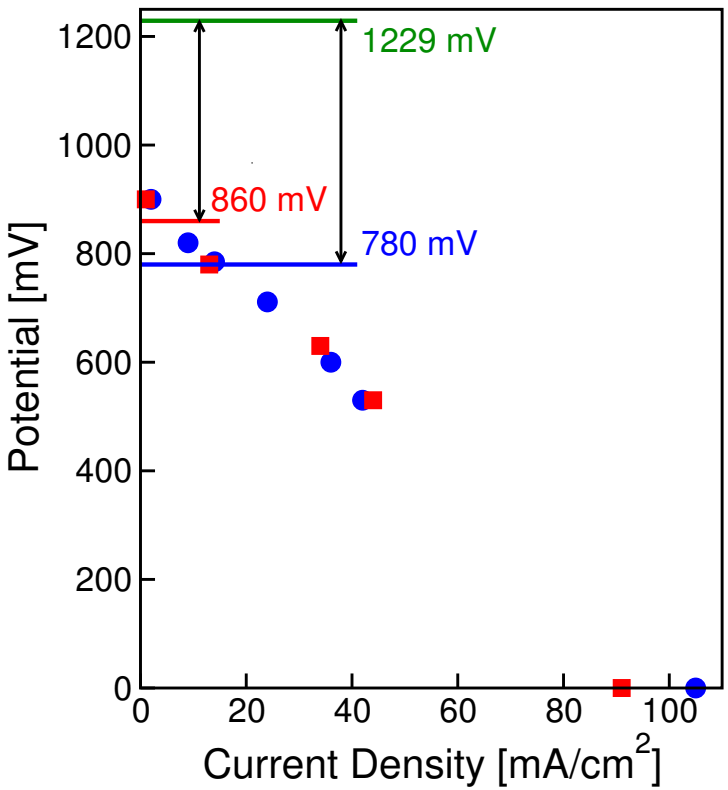

PtNi/Pd has higher open circuit voltage, similar performance to Pt/Pd.

Fuel cell performance and open questions

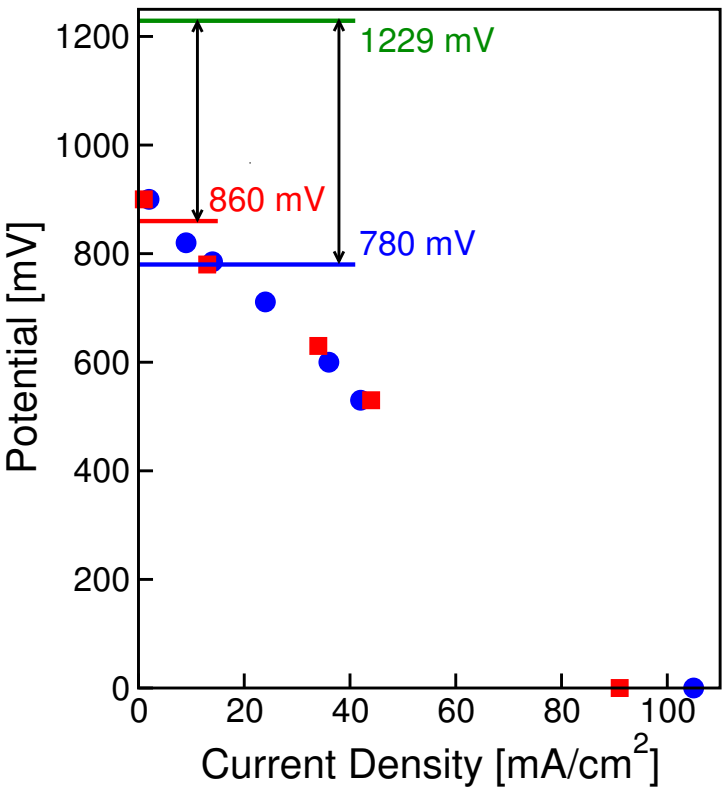

PtNi/Pd has higher open circuit voltage, similar performance to Pt/Pd.

Pt: How do reactants adsorb on platinum surface?

- Do all faces of Pt adsorb equally well?
- Is there a change in location with coverage?

PtNi: Why is ORR improved with bimetallic catalyst?

- Pt electronic structure modified
- Pt catalyst geometric structure modified
- Static oxygen adsorbates inhibited
- Overpotential reduced

How do real catalysts differ from model systems?

Pt/C and PtNi/C comparison

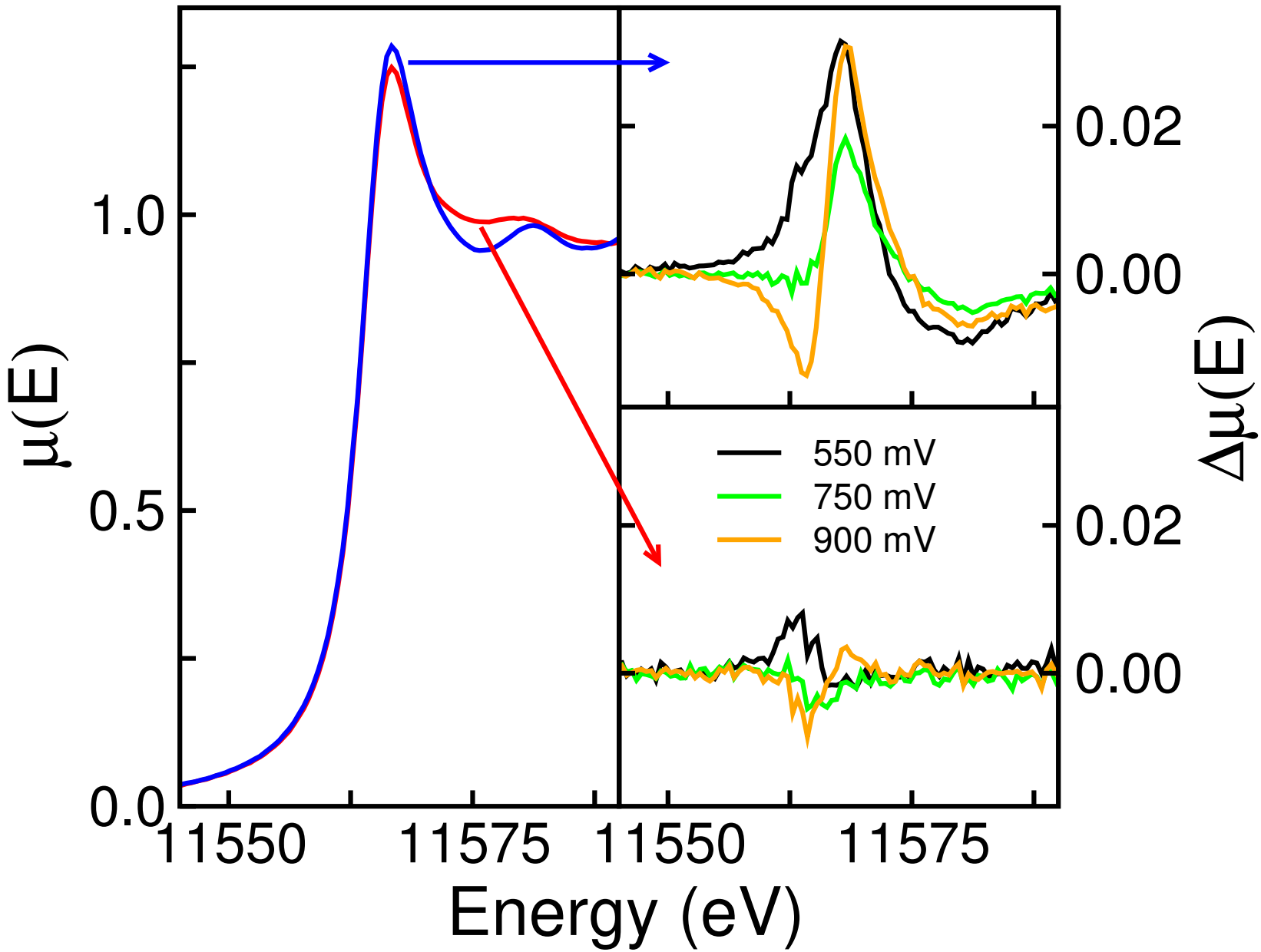

PtNi structural model

Attempt to get global information about the oxygen

Fit all potentials with same metal core parameters for each catalyst

Simultaneous fit of Pt and Ni edges in PtNi/C with constraint on Pt-Ni distance

Fit in k, k^2, and k^3 weighting simultaneously

M-O path constraints

- length common across potentials
- σ^2fixed to 0.01
- Pt-O in PtNi/C are refined with a single occupation #

Example fits

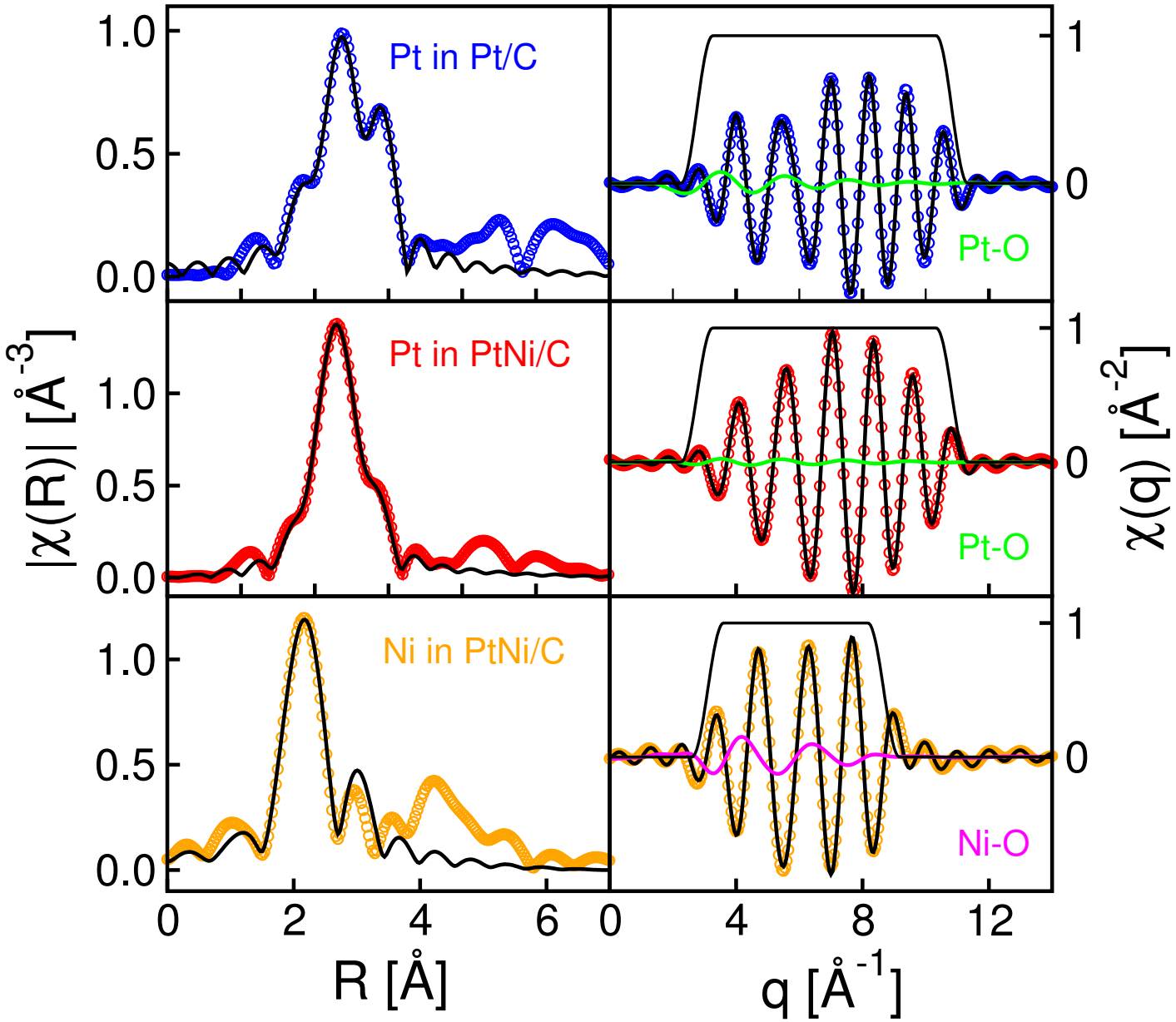

Fit results

Pt/C		PtNi/C			
		Pt		Ni	
N_{Pt}	8.7 ± 0.2	N_{Pt}	6.1 ± 0.3	N_{Ni}	3.7 ± 0.2
$R_{Pt\text{-}Pt}$	2.749 ± 0.001	$R_{Pt\text{-}Pt}$	2.692 ± 0.003	$R_{Ni\text{-}Ni}$	2.572 ± 0.006
		N_{Ni}	3.4 ± 0.1	N_{Pt}	8.9 ± 0.5
		$R_{Pt\text{-}Ni}$		2.635 ± 0.004	
		N_{Total}	9.5 ± 0.4	N_{Total}	12.6 ± 0.7
$R_{Pt\text{-}O}$	2.02 ± 0.01	$R_{Pt\text{-}O}$	2.09 ± 0.03	$R_{Ni\text{-}O}$	1.90 ± 0.01

Note the Pt-Pt and Pt-O bond lengths as well as total metal near neighbors

What does Ni really do?

Resides predominantly in metal core of nanoparticle

Eliminates static Pt-O bonds at all potentials

Number of O near neighbors "increases" with potential

Lengthens Pt-O and shortens Pt-Pt bond

Reduces Pt white line in most reduced state (0 mV)

Open circuit voltage is increased (reduction in overpotential)

Can we use modeling to establish specific mechanism?

- Pt-Pt bond reduction (weakening of Pt-O bond)?
- Electron donation to Pt d-band (weakening of Pt-O bond)?
- Stronger affinity for oxygen?

Pt cluster modeling

By using FEFF8.4, which performs full multiple-scattering self-consistent calculations, we can explore the implications of the "ligand effect" and the "strain effect" on the electronic state of Pt.

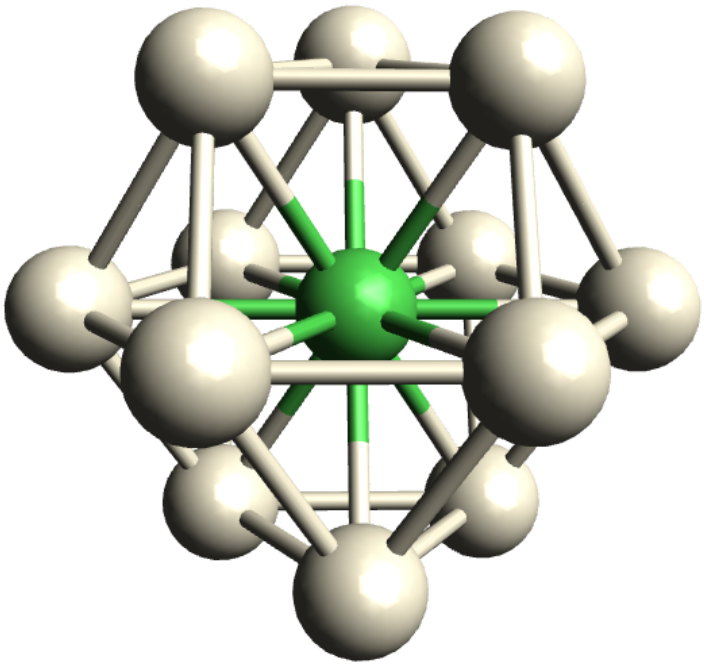

Separate the effects of

(a) Shorter Pt-Pt distance

(b) charge transfer from subsurface Ni

Use experimentally determined distances

Calculate local density of states

Calculate XANES spectrum

Q. Jia, et al., "Structure-property-activity correlations of Pt-bimetallic nanoparticles: a theoretical study" *Electrochimica Acta* bf 88, 604 (2013).

Cluster calculation results

Strain effect: shorter Pt-Pt bond $\rightarrow$ broader and lower Pt d-band

- serves to weaken the Pt-O bond
- White line at absorption edge is reduced
- In agreement with DFT calculations (Nørskov et al.)

Ligand effect: subsurface Ni $\rightarrow$ sharpens and raises Pt d-band

- Raises chemisorption energy
- Increases white line

Net effect dominated by strain effect

Predictive ability

- Moving down periodic table (Ru, Ag)
- Moving left across periodic table (towards Mn)

Methanol oxidation by a PtRu anode

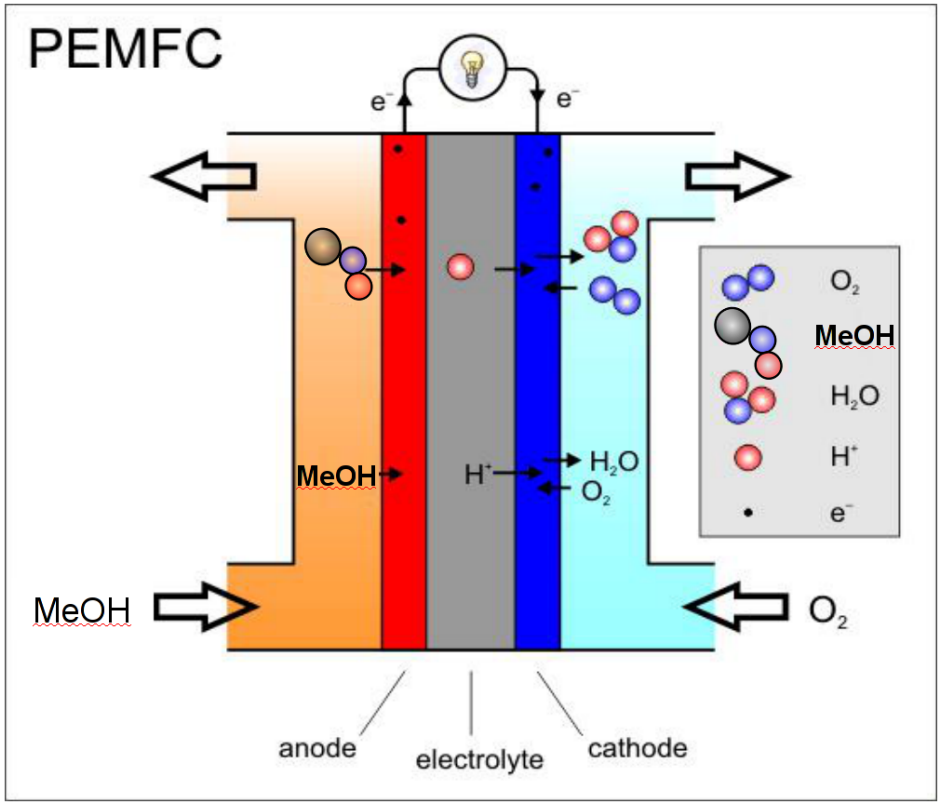

U.S. Department of Defense (DoD) Fuel Cell Test and Evaluation Center (FCTec)

Anode: 0.02 V vs. SHE

$$CH_3OH + H_2O \longrightarrow 6\,H + CO_2 + 6\,e^-$$

Cathode: 1.23 V s. SHE

$$\frac{3}{2}\,O_2 + 6\,H^+ + 6\,e^- \longrightarrow 3\,H_2O$$

Pt surface poisoned by CO

The presence of Ru promotes CO oxidation through a "bi-functional mechanism"

$$Pt{-}(CO)_{ads} + Ru{-}OH \longrightarrow Pt + RuCO_2 + H^+ + 2\,e^-$$

Ru EXAFS fitting

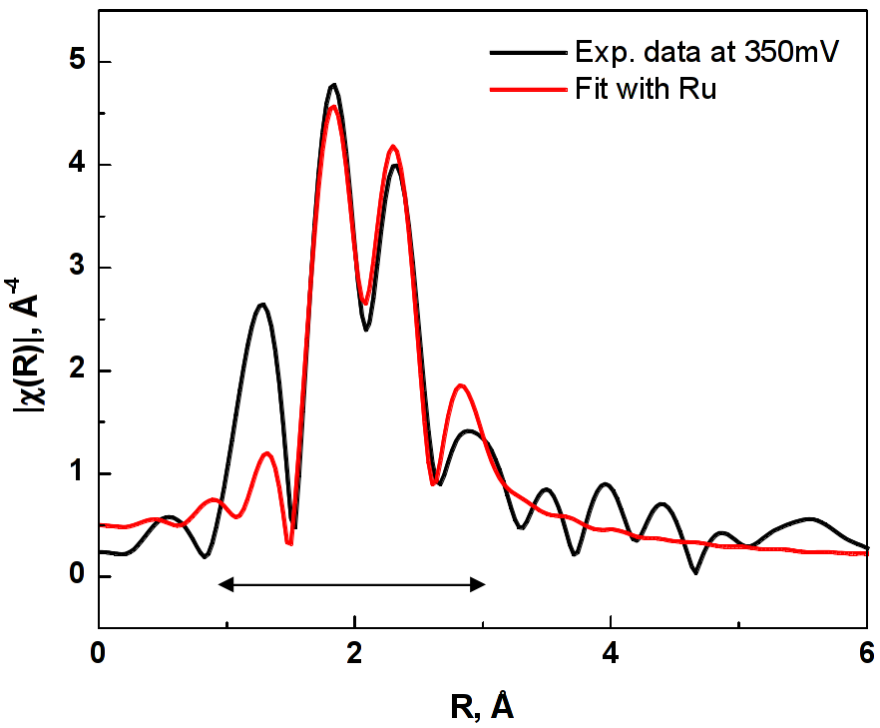

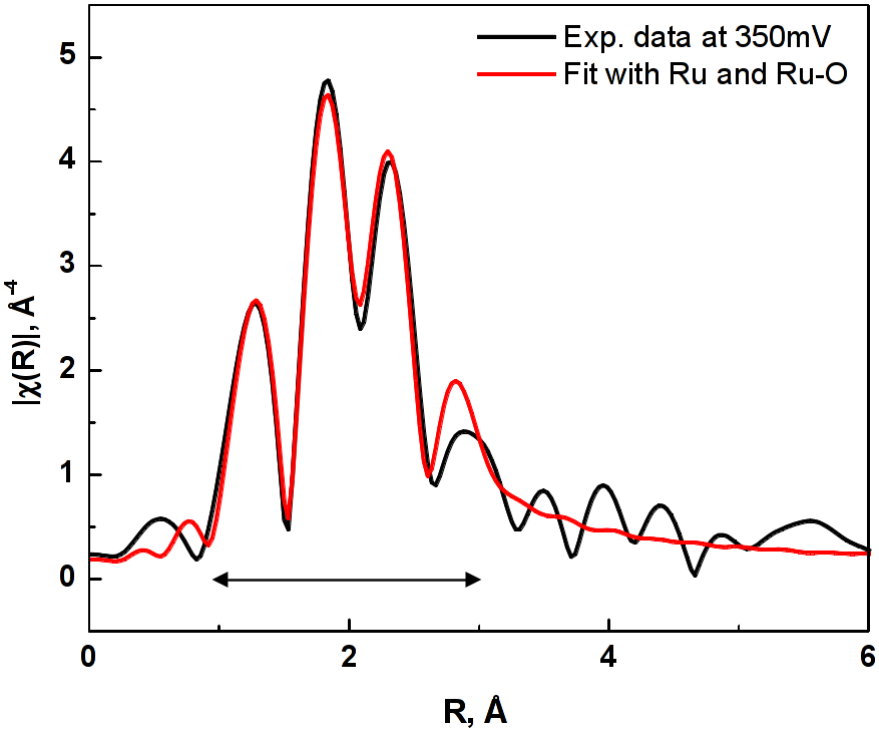

- Addition of Ru-O/C neighbors improves the EXAFS fit
- The peak at about 1.3 Å is ascribed to oxygen bound to Ru
- The asymmetric distribution of the Ru-O/C peak is consistent with disorder

Metal nanoparticle structure

- First shell analysis
- Fit Pt and Ru EXAFS simultaneously at each potential. No potential dependence observed
- Simultaneously fit Pt and Ru data at all potentials. Identical overall average coordination was observed
- Use fractional coordination numbers, x (Pt around Ru) and y (Ru around Pt) and total coordination number about each atom, N
- Bond lengths and Debye-Waller factors are consistent with literature values for C supported Pt-Ru catalyst (Russel 2001, Camara 2002)

N	8.2 ± 0.2
x	0.54 ± 0.02
y	0.27 ± 0.02

$$\frac{[Ru]}{[Pt]} = \frac{y}{x} = 0.50$$

Metal core restucturing

As-received catalyst

Ru oxidation ~ 58 %

N = 5.6

$$\frac{[Ru]}{[Pt]} = \frac{y}{x} = 0.44$$

Pt-O bonds present

Ru-O bonds $\sim$2.8

In-situ catalyst

Ru oxidation ~ 15 %

N = 8.2

$$\frac{[Ru]}{[Pt]} = \frac{y}{x} = 0.50$$

No Pt-O bonds

Ru-O/C bonds $\sim$0.24

- Inner core has more Pt than Ru
- Ru on surface and outside of metallic nanoparticle

S. Stoupin, et al., "Pt and Ru X-ray absorption spectroscopy of PtRu anode catalysts in operating direct methanol fuel cells" *J. Phys. Chem.* **110**, 9932 (2006).

S. Stoupin, et al., "Structural analysis of sonochemically prepared PtRu versus Johnson Matthey PtRu in operating direct methanol fuel cells" *Phys. Chem. Chem. Phys.* **10**, 6430 (2008).

Role of Ru in CO oxidation?

- PtRu bifunctional catalyst improves performance
- In commercial PtRu catalysts there is always a lot of inactive Ru-oxide (?)
- Ru signal dominated by metallic Ru environment
- How does Ru behave in the presence of reactants adsorbed on platinum surface?

Core-shell nanoparticles can resolve these questions

Ru-decorated Pt nanoparticles

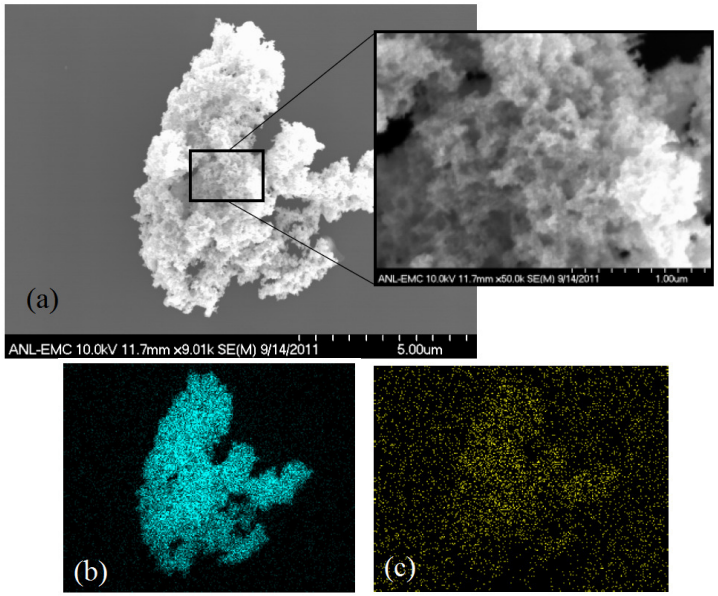

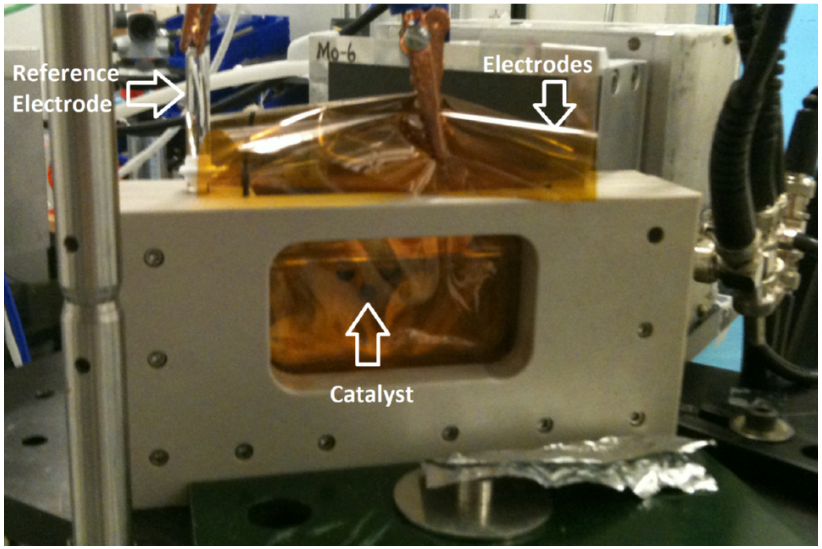

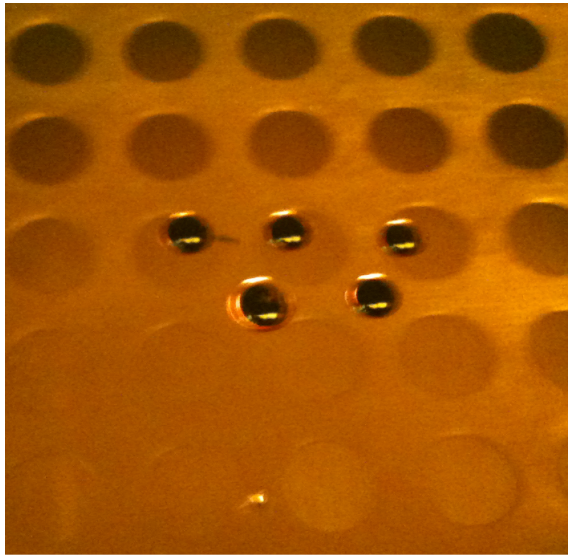

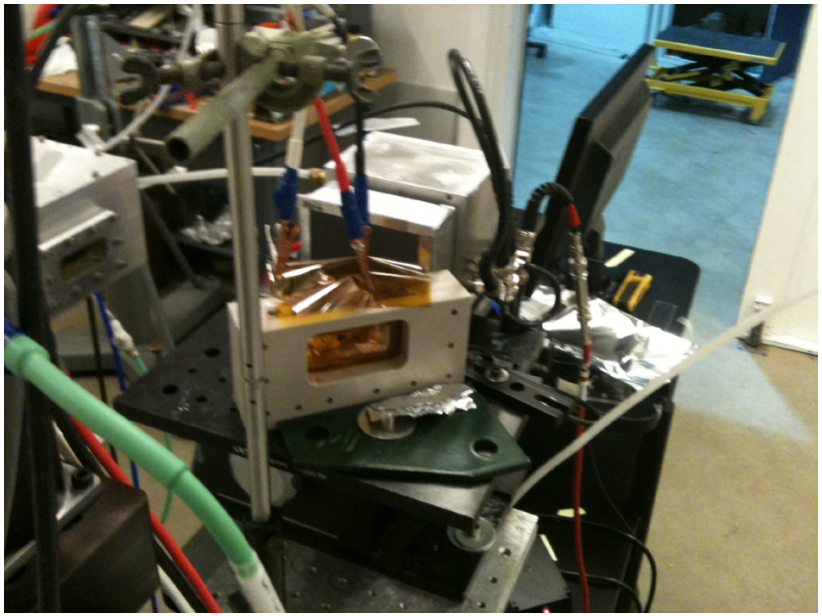

Electrochemical performance

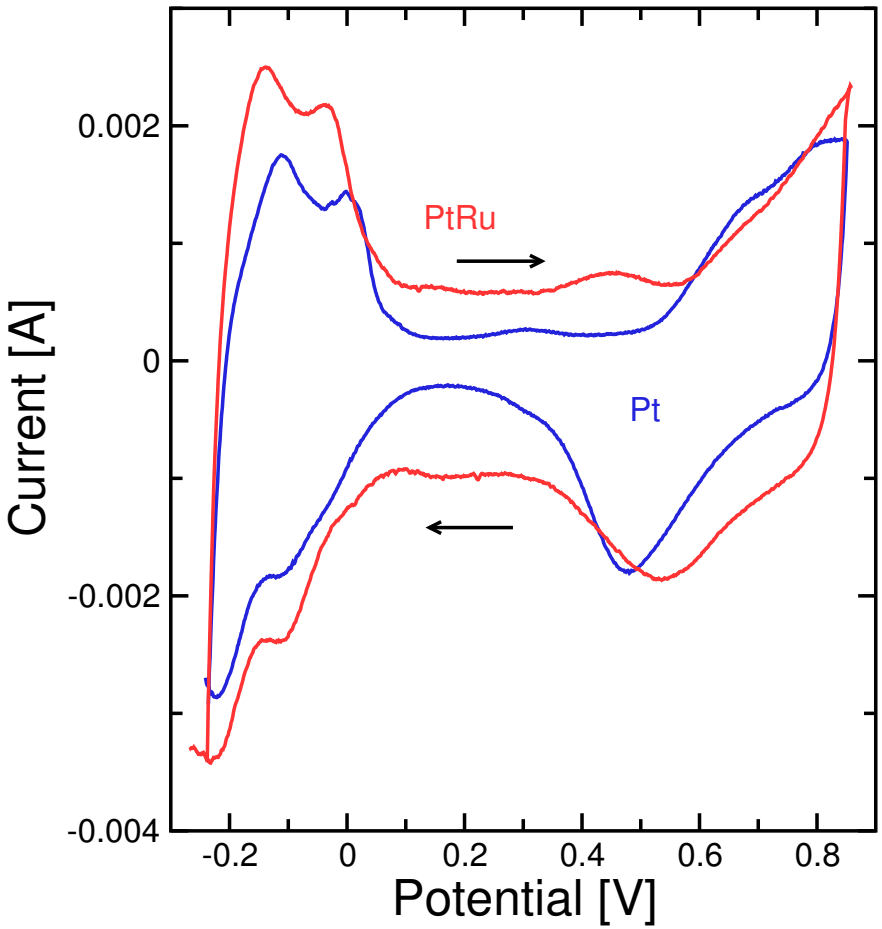

Without Methanol

Low V peaks are H^+ stripping

Dip at $\sim$0.5 V is oxygen stripping

Ru shifts potential on all peaks

Electrochemical performance

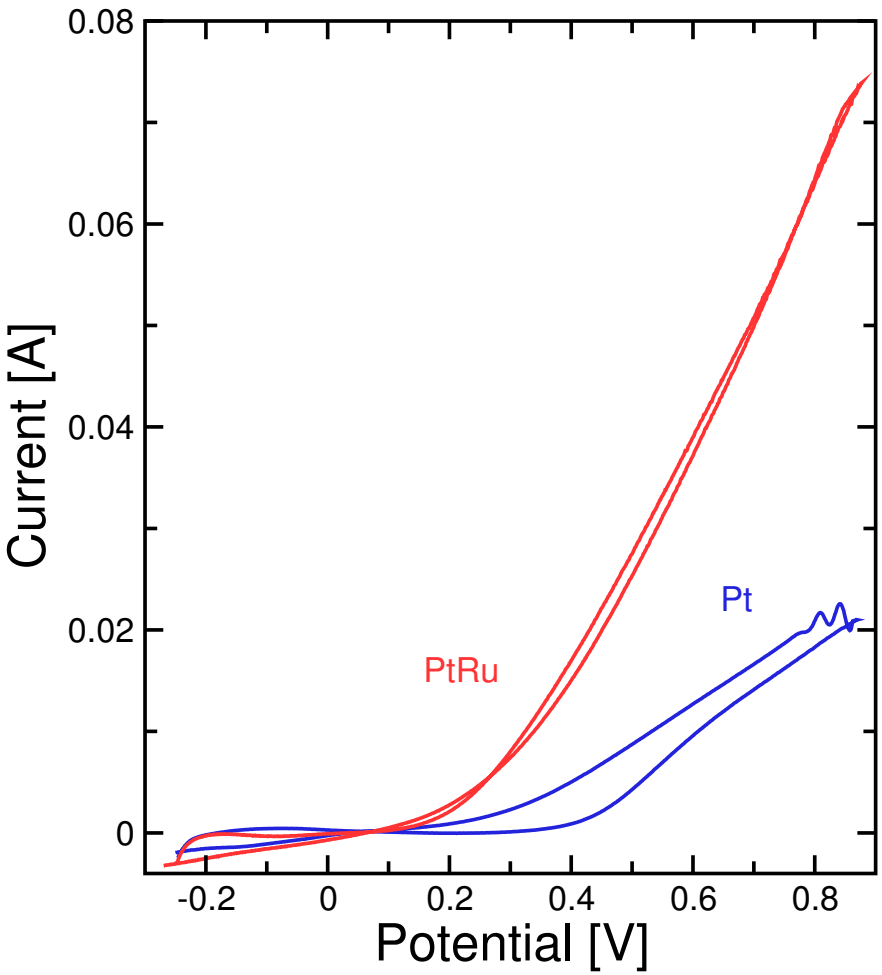

Without Methanol

Low V peaks are H^+ stripping

Dip at $\sim$0.5 V is oxygen stripping

Ru shifts potential on all peaks

With Methanol

Continual current growth is due to methanol oxidation

Ru improves current by removing the CO which blocks active sites

Ru EXAFS

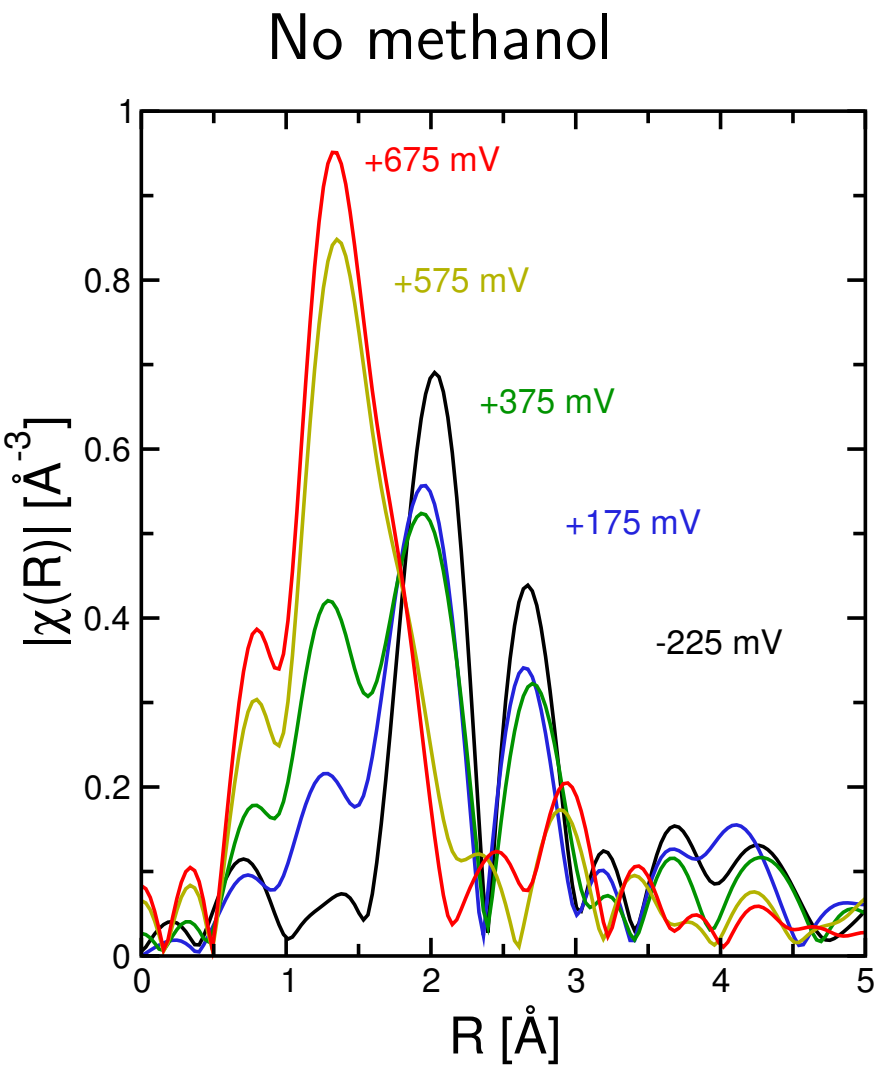
No methanol
+675 mV
+575 mV
+375 mV
+175 mV
-225 mV
|χ(R)| [Å^-3]
R [Å]
0
0.2
0.4
0.6
0.8
1
0
1
2
3
4
5

Ru EXAFS

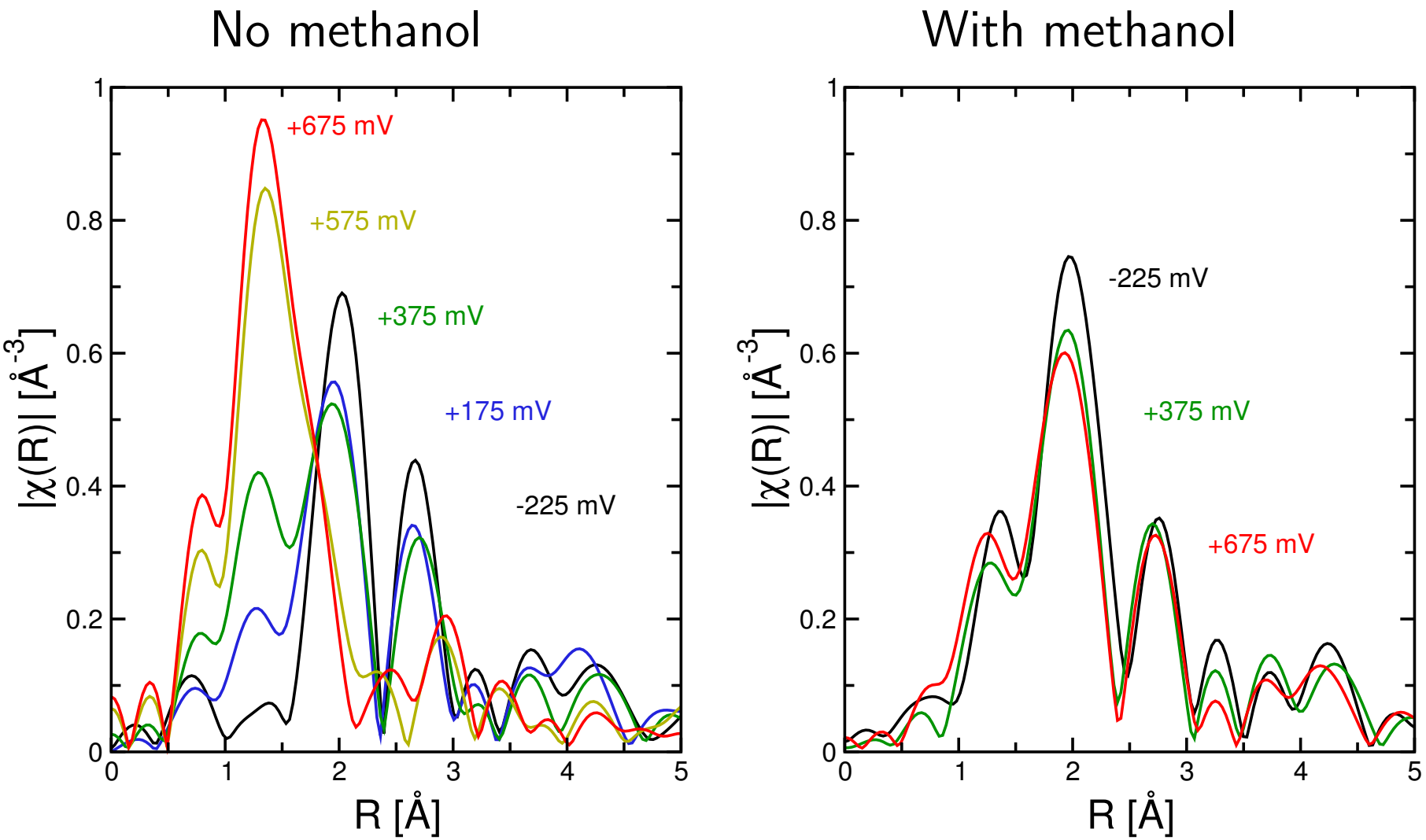
No methanol
+675 mV
+575 mV
+375 mV
+175 mV
-225 mV
|χ(R)| [Å^-3]
R [Å]
With methanol
-225 mV
+375 mV
+675 mV
|χ(R)| [Å^-3]
R [Å]

Ru-M paths

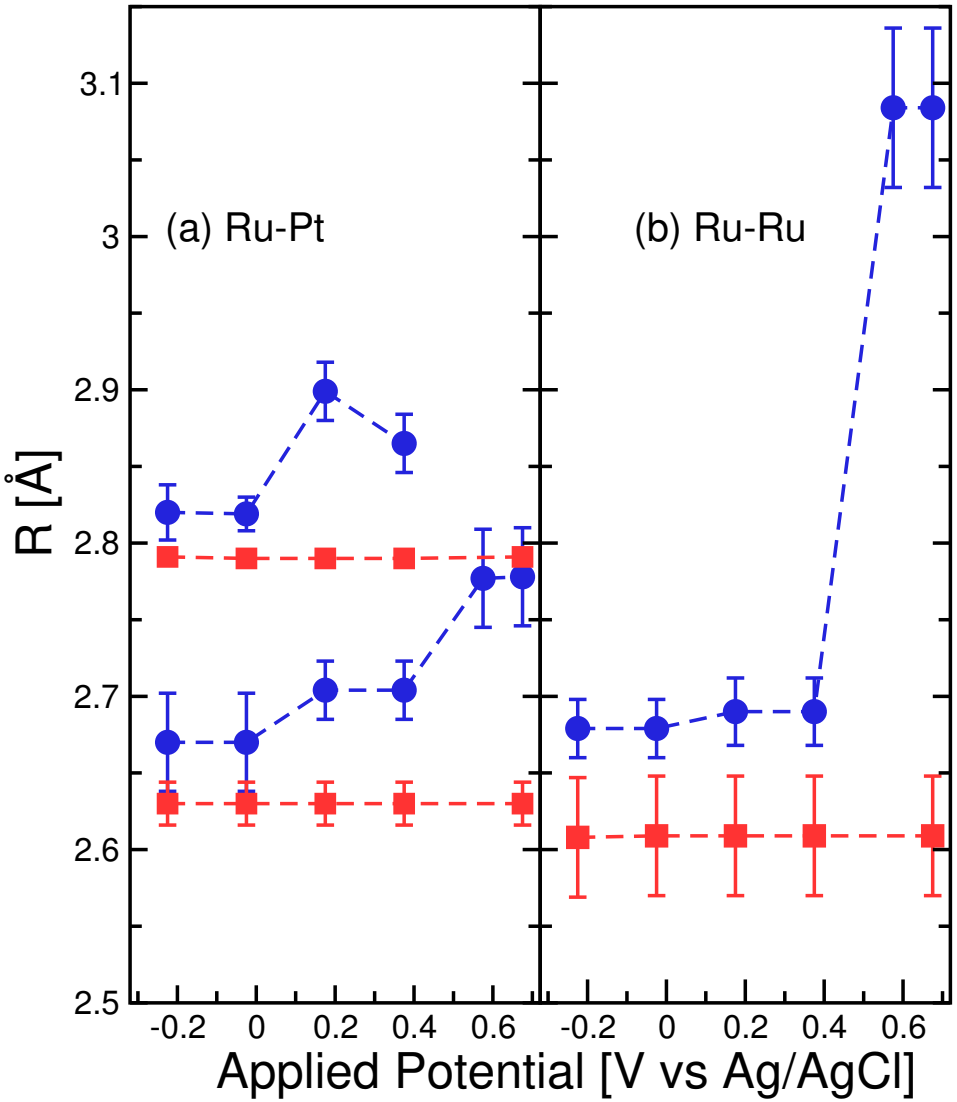

Without methanol

With methanol

Ru-M paths

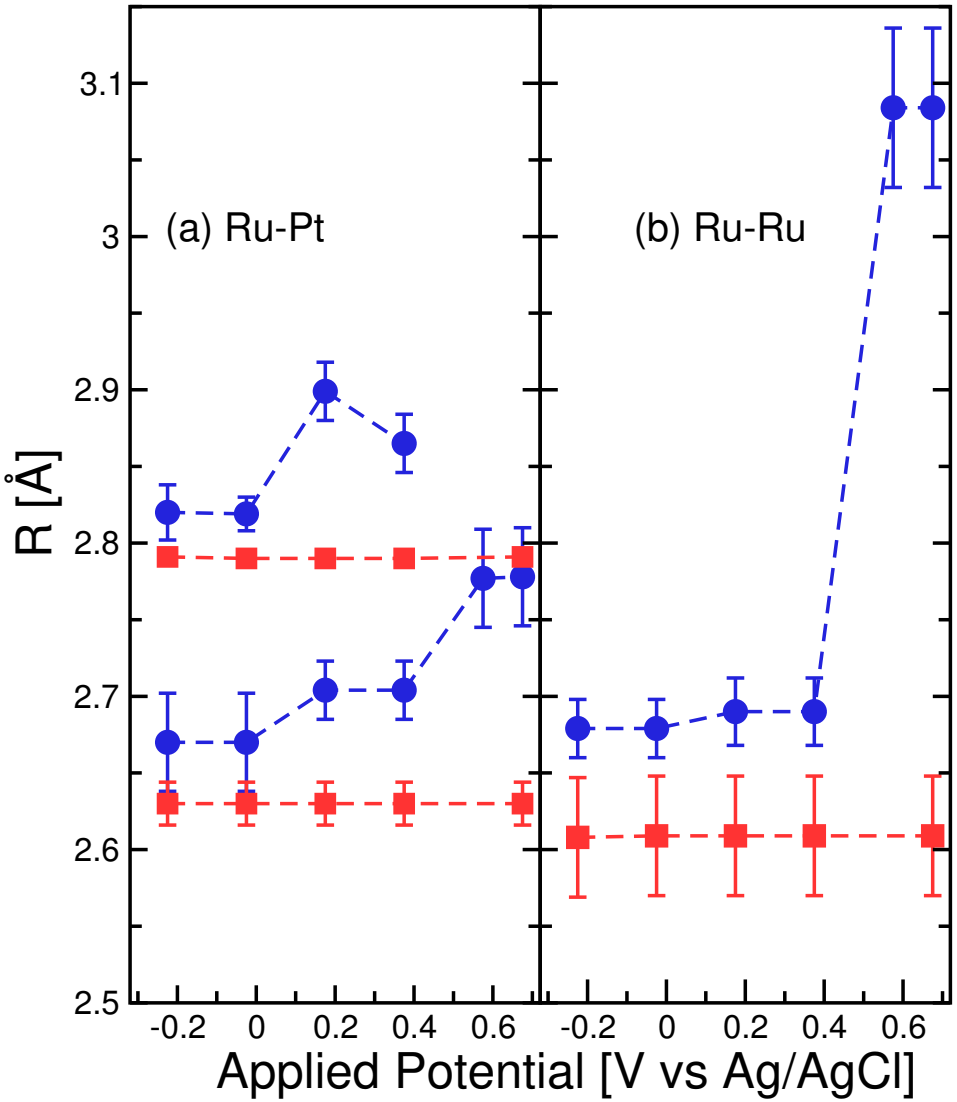

Without methanol

Ru-M distances are longer and RuO_2 is formed at high potentials

With methanol

Ru-M paths

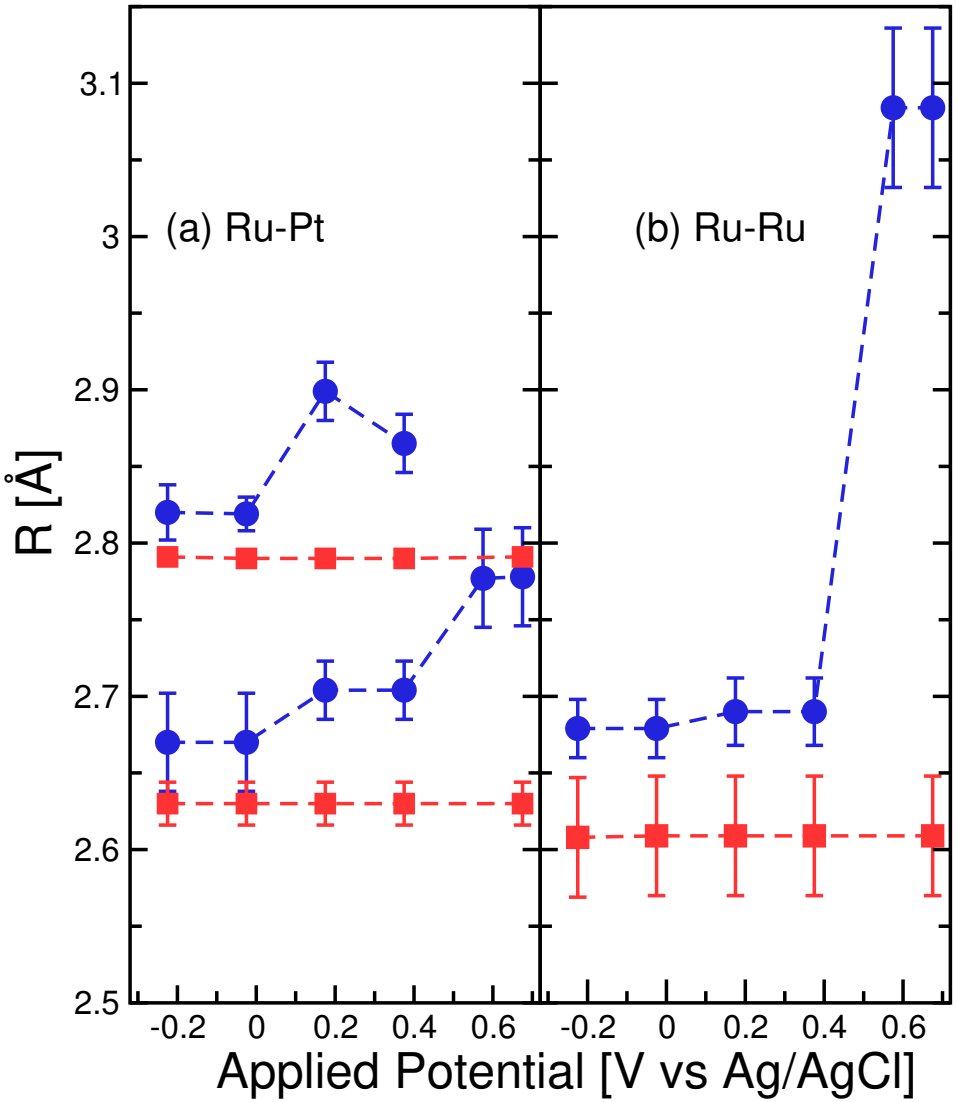

Without methanol

Ru-M distances are longer and RuO_2 is formed at high potentials

With methanol

Ru-M distances are shorter and remain the same at all potentials

Ru-O/C paths

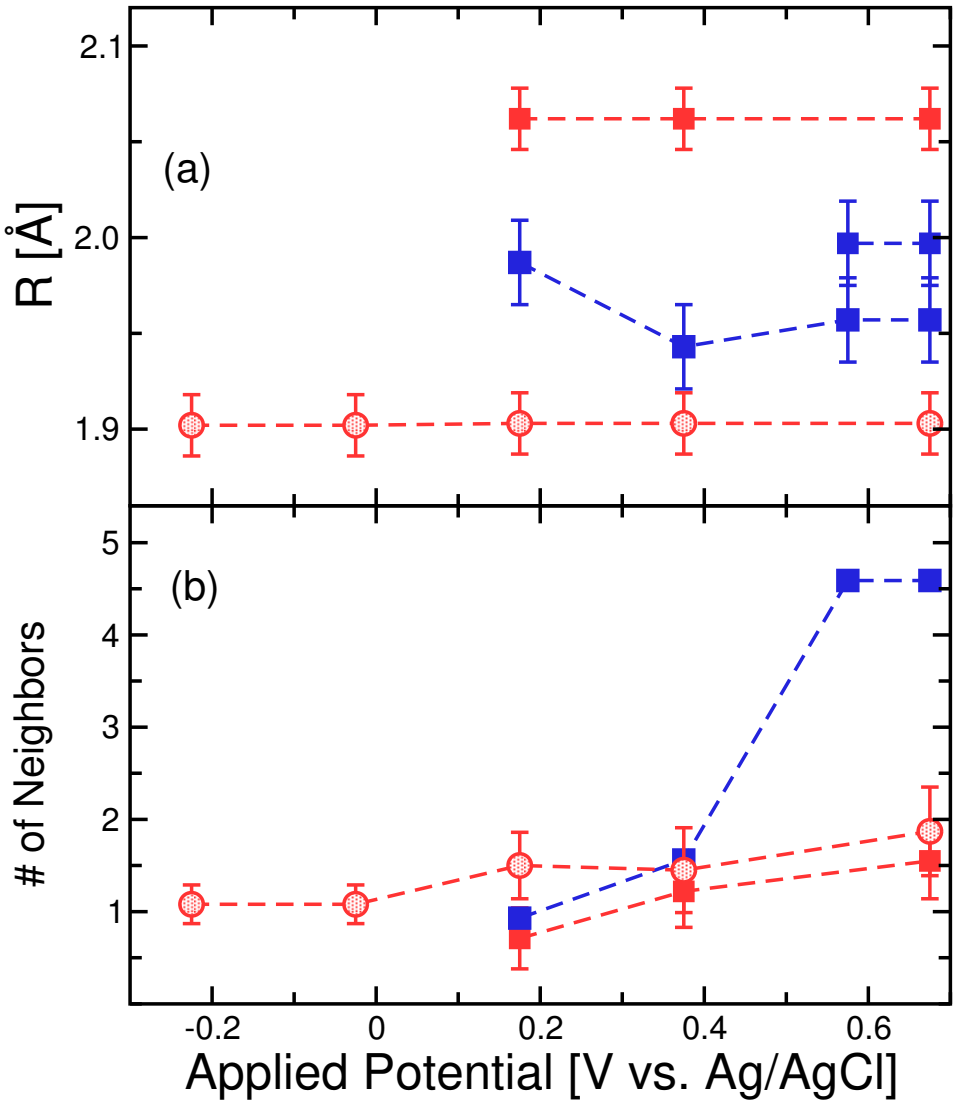

Without methanol

With methanol

Ru-O/C paths

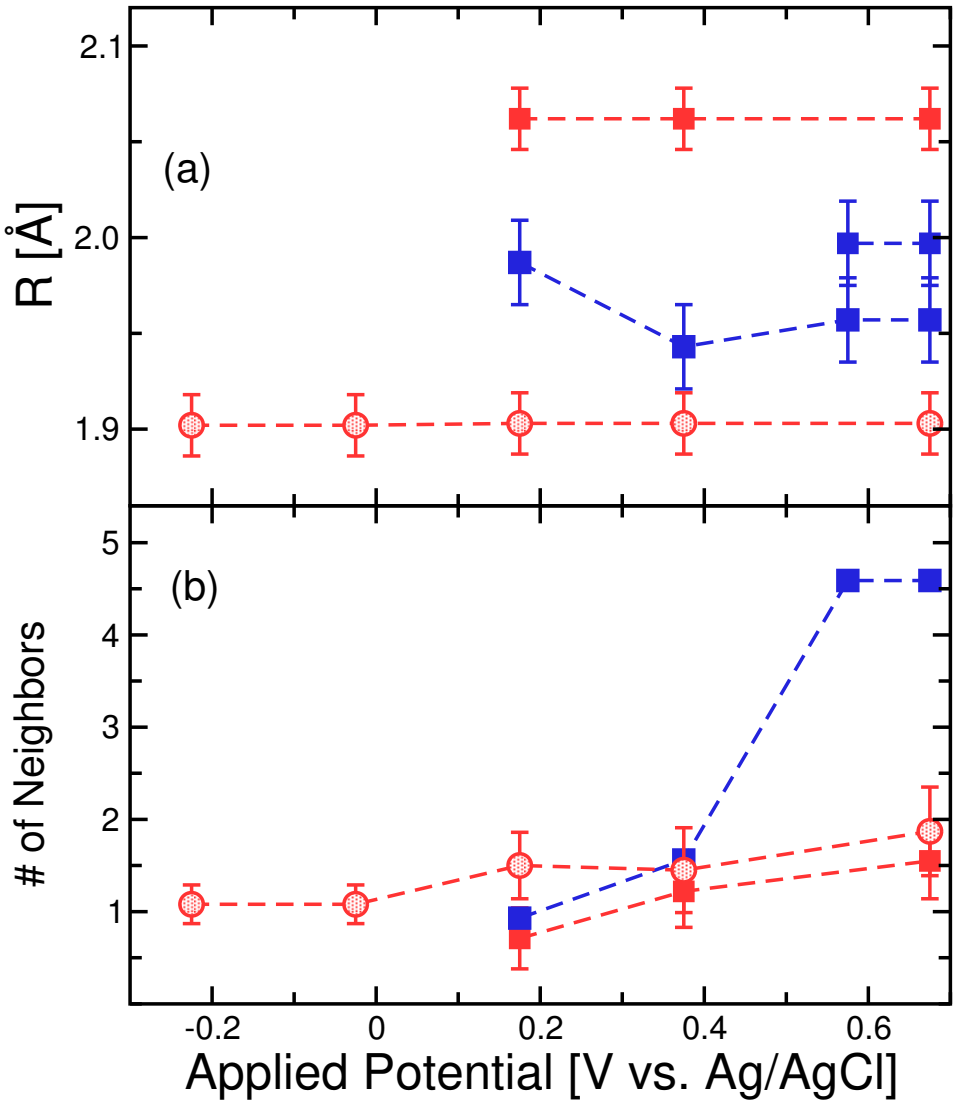

Without methanol

Above 375 mV Ru-O paths appear and total number of Ru-O neighbors increases to that of RuO_2

With methanol

Ru-O/C paths

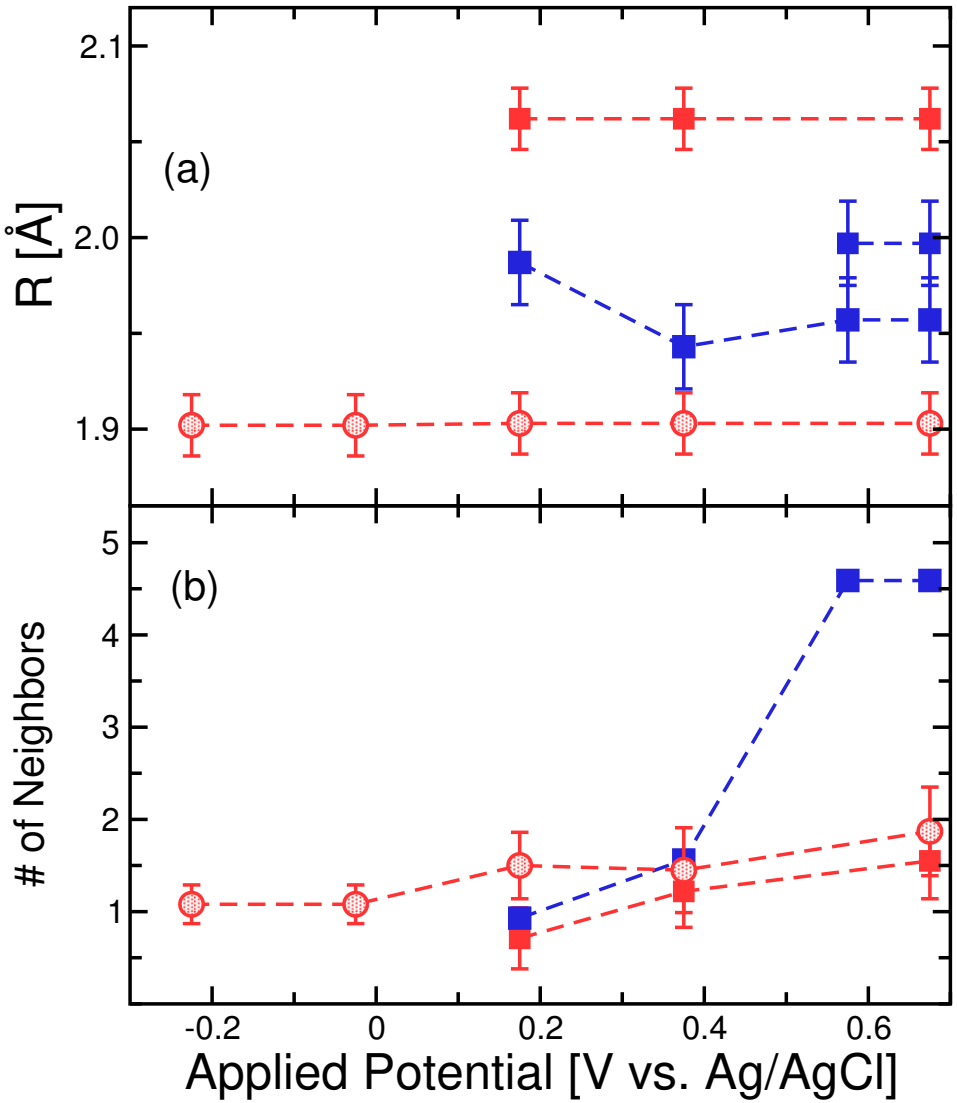

Without methanol

Above 375 mV Ru-O paths appear and total number of Ru-O neighbors increases to that of RuO_2

With methanol

Ru has one low Z neighbor at all potentials (carbon); a second above 175 mV (oxygen) with constant bond lengths and slightly increasing numbers

Bi-functional mechanism

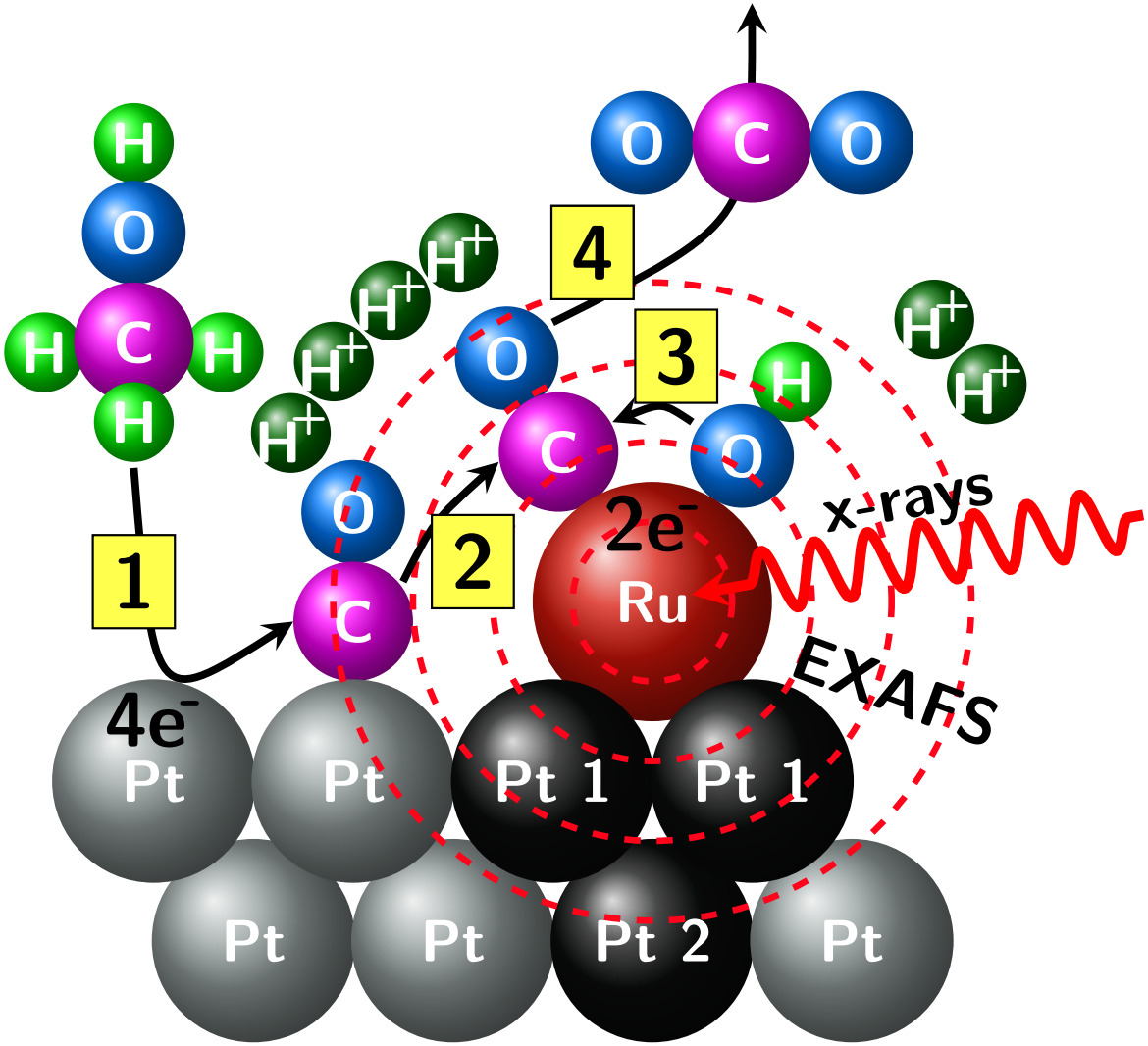

C. Pelliccione et al., "In situ Ru K-Edge x-ray absorption spectroscopy study of methanol oxidation mechanisms on model submonolayer Ru on Pt nanoparticle electrocatalyst" *J. Phys. Chem.* **C 117**, 18904 (2013).